



Published in final edited form as:

Nat Cardiovasc Res. 2022 March ; 1(3): 253–262. doi:10.1038/s44161-022-00023-x.

The pleiotropic benefits of statins include the ability to reduce CD47 and amplify the effect of pro-efferocytic therapies in atherosclerosis

Kai-Uwe Jarr¹, Jianqin Ye¹, Yoko Kojima¹, Zhongde Ye¹, Hua Gao¹, Sofie Schmid², Lingfeng Luo¹, Richard A. Baylis¹, Mozghan Lotfi¹, Nicolas Lopez¹, Anne V. Eberhard¹, Bryan Ronain Smith^{3,4}, Irving L. Weissman⁵, Lars Maegdefessel^{2,6,7}, Nicholas J. Leeper^{1,8,9}

¹Department of Surgery, Division of Vascular Surgery, Stanford University School of Medicine, Stanford, California, United States of America.

²Department for Vascular and Endovascular Surgery, Klinikum rechts der Isar, Technical University Munich, Munich, Germany.

³Department of Biomedical Engineering, Michigan State University, East Lansing, Michigan, United States of America.

⁴Institute for Quantitative Health Science and Engineering, East Lansing, Michigan, United States of America.

⁵Stanford Institute for Stem Cell Biology and Regenerative Medicine, Stanford University, Stanford, California, United States of America.

⁶German Center for Cardiovascular Research, Berlin, Germany (DZHK partner site Munich Heart Alliance).

⁷Department of Medicine, Karolinska Institute, Stockholm, Sweden.

⁸Stanford Cardiovascular Institute, Stanford University, Stanford, California, United States of America.

⁹Department of Medicine, Division of Cardiovascular Medicine, Stanford University School of Medicine, Stanford, California, United States of America.

Abstract

Users may view, print, copy, and download text and data-mine the content in such documents, for the purposes of academic research, subject always to the full Conditions of use: <https://www.springernature.com/gp/open-research/policies/accepted-manuscript-terms>

Corresponding Author: Nicholas J. Leeper, MD, Divisions of Vascular Surgery and Cardiovascular Medicine, Stanford University, 300 Pasteur Drive, Room H3638, Stanford, CA 94305, USA. nleeper@stanford.edu. Phone: +1-650-725-5227.

Author Contributions

K.-U.J., J.Y., Y.K., Z.Y., H.G., L.L., S.S., M.L., N.L., A.V.E. conducted experiments, and collected and analysed data. K.-U.J., J.Y., Y.K., Z.Y., H.G., L.L., R.A.B., B.R.S., I.L.W., L.M., and N.J.L. conceptualized and designed experiments, discussed results, and interpreted data. K.-U.J. and N.J.L. designed figures and wrote the manuscript. K.-U.J. directed the study. N.J.L. supervised the study.

Competing Interests

I.L.W. and N.J.L. are co-founders and directors of Bitterroot Bio Incorporated, a cardiovascular company studying macrophage checkpoint inhibition. K.-U.J., Y.K., I.L.W., and N.J.L. have filed a provisional patent (U.S. Application Serial No. 63/106,794): 'CD47 Blockade and Combination Therapies Thereof For Reduction Of Vascular Inflammation'. The remaining authors declare no competing interests.

The pleiotropic benefits of statins may result from their impact on vascular inflammation. The molecular process underlying this phenomenon is not fully elucidated. Here, RNA sequencing designed to investigate gene expression patterns following CD47-SIRP α inhibition identifies a link between statins, efferocytosis, and vascular inflammation. In vivo and in vitro studies provide evidence that statins augment programmed cell removal by inhibiting the nuclear translocation of NF κ B1 p50 and suppressing the expression of the critical ‘don’t eat me’ molecule, CD47. Statins amplify the phagocytic capacity of macrophages, and thus the anti-atherosclerotic effects of CD47-SIRP α blockade, in an additive manner. Analyses of clinical biobank specimens suggest a similar link between statins and CD47 expression in humans, highlighting the potential translational implications. Taken together, our findings identify efferocytosis and CD47 as pivotal mediators of statin pleiotropy. In turn, statins amplify the anti-atherosclerotic effects of pro-phagocytic therapies independently of any lipid-lowering effect.

Keywords

Atherosclerosis; Statin; Pleiotropy; CD47; Efferocytosis

Introduction

Atherosclerosis is a lipoprotein-driven, inflammatory process underlying heart attack and stroke, and is the leading cause of death worldwide¹. In the last four decades, 3-hydroxy-3-methylglutaryl coenzyme A (HMG-CoA) reductase inhibitors, known as statins, have been established as the drug of first choice for patients with atherosclerotic cardiovascular disease. Striking data from multiple clinical trials have shown that they reduce mortality in both primary and secondary prevention^{2,3}. Statins inhibit the rate-limiting enzyme of cholesterol biosynthesis and reduce serum low-density lipoprotein (LDL) cholesterol, thus directly addressing one of the most important risk factors for the disease.

However, there is growing evidence that the beneficial properties of statins are not restricted to their influence on LDL. Indeed, the so-called pleiotropic effects of statins are now well described^{4,5}, and may result from their impact on vascular inflammation^{6,7}. This possibility has garnered attention due to a series of recent high profile studies, including CANTOS (which used a monoclonal antibody directed against the interleukin-1 β pathway) and COLCOT (which used colchicine to target tubulin polymerization, microtubule generation, and possibly the inflammasome), which helped definitively prove the ‘inflammatory hypothesis of atherosclerosis’⁸. These large clinical trials are spurring the concept of targeting inflammation as a way to provide benefit independently of lipid levels^{9,10}.

A critical driver of inflammation is the accumulation of diseased and dying macrophages and smooth muscle cells in the atherosclerotic vessel. Normally, these pathological cells would be identified for phagocytic removal by macrophages in the plaque. In keeping with Peter Henson’s suggestion, the term ‘efferocytosis’ is used to emphasize the relevance of this process (derived from the Latin verb ‘*efferre* – *effero*’, meaning to bury, or to carry to the grave). However, this process is defective in atherosclerosis, due in part to the pathological upregulation of a so-called ‘don’t eat me’ molecule known as

CD47¹¹. The presence of this anti-phagocytic signal has been hypothesized to permit the accumulation of inflammatory debris in the necrotic core and therefore promote lesion expansion. Mechanistically, CD47 binds to signal-regulatory protein alpha (SIRP α), a transmembrane protein with an immunoreceptor tyrosine-based inhibitor motif domain. Ligation of SIRP α leads to tyrosine phosphorylation and subsequent activation of the Src homology 2 domain-containing phosphatase-1 (SHP-1), which inhibits phagocytosis¹¹. Preclinical studies using antibodies directed against CD47 or nanoparticles targeting SHP-1 led to reactivation of intraplaque efferocytosis and prevention of atherosclerosis, supporting a causal relationship^{11–13}. Additionally, we provided the first evidence that a humanized anti-CD47 antibody could reduce arterial ¹⁸F-fluorodeoxyglucose uptake, detected by positron-emission tomography and computed tomography, and thus suppress vascular inflammation in patients¹⁴. Although these preliminary observations require confirmation in a prospective trial, pro-efferocytic therapies are hypothesized to represent a new strategy to target inflammation in cardiovascular disease.

In this study, we describe how an unbiased approach designed to investigate gene expression patterns in response to CD47-SIRP α blockade led to a surprising link between statins and efferocytosis. We provide the first evidence that statins may amplify the anti-atherosclerotic effects of CD47-SIRP α blockade, due to an NF κ B1-dependent alteration in ‘don’t eat me’ molecule expression, which occurs independent of any effect on lipid levels. When coupled with supporting clinical data from patients with atherosclerotic cardiovascular disease, these findings not only provide insights into the mechanistic origins of statin pleiotropy, but also provide a basis for future translational efforts focused on therapies which may synergize with evidence-based medicines to further reduce the risk of major adverse clinical events.

Results

Statin as top upstream regulator of SHP-1 inhibition

As an unbiased approach, RNA sequencing was used to examine the transcriptome of macrophages after CD47-SIRP α axis blockade. Therefore, bone marrow-derived macrophages were incubated with single-walled carbon nanotubes loaded with fluorescent Cy5.5 probe (referred to as SWNT) or SWNT loaded with a small-molecule inhibitor of SIRP α ’s downstream effector molecule SHP-1 (referred to as SHP1i) for 24 hours, and sorted by flow cytometry to isolate Cy5.5-positive macrophages in each group, which were then subjected to RNA sequencing (Extended Data Figure 1a). Here, we identified 128 differentially expressed genes with a false-discovery rate of less than 0.10 (19 up-regulated and 109 down-regulated) in this study (Figure 1a and Extended Data Table 1).

We next identified ‘upstream regulators’ using Qiagen’s Ingenuity Pathway Analysis. Intriguingly, lovastatin, a first generation HMG-CoA reductase inhibitor, was one of the top activated upstream regulators and the only drug in the database (z-score 2.184), based on the relevant regulation of apolipoprotein E, ras homolog family member B, RB transcriptional corepressor like 1, glutathione peroxidase 3, and X-linked inhibitor of apoptosis (Figure 1b – 1c and Extended Data Table 2). In anticipation of our *in vivo* model, we validated these findings for atorvastatin, the most widely prescribed statin with one of the most favourable safety profiles¹⁵, by quantitative polymerase chain reaction. We found

similar gene expression changes upon atorvastatin treatment (Extended Data Figure 1b). In conclusion, these data suggested an unexpected overlap of HMG-CoA reductase inhibition and CD47-SIRP α blockade.

Effect of CD47 blockade and atorvastatin on atherosclerosis

The unanticipated crosstalk and the resulting emerging translational potential prompted us to test whether combined treatment of CD47-SIRP α blockade and HMG-CoA reductase inhibition has additive effects on the atherosclerotic plaque activity *in vivo*. To address this question, high-fat diet-fed Apoe^{-/-} mice received therapy with atorvastatin alone or in combination with CD47-SIRP α blockade (Extended Data Figure 2a – 2i). The latter was achieved by targeting either CD47 (using anti-CD47 antibodies¹¹) or SIRP α 's downstream effector molecule SHP-1 (using SHP1i¹³). Intriguingly, combined treatment not only decreased lesion size but also reduced necrotic core area (Figure 2a – 2b and Extended Data Figure 2j). This is important to note, given that the necrotic core is thought to be a key driver for plaque vulnerability in lesions and thus for acute vascular events¹⁶. Of note, there were no significant differences in plasma cholesterol and blood glucose between the cohorts (Figure 2c). Subsequently, we used the single treatment cohorts to determine additivity/synergy of compounds (Extended Data Figure 2k – 2l). Applying the Bliss independence model (formula $E_c = E_a + E_b - E_a \cdot E_b$, where E_c is the combined effect produced by the combination of compounds a and b)¹⁷ on the analyses of lesion area and necrotic core size, we computed an additive anti-atherosclerotic effect for both parameters *in vivo* (Figure 2d – 2e). Together, these observations suggested an additive therapeutic effect upon combination.

Effect of CD47 blockade and atorvastatin on efferocytosis

Given that the efficient clearance of apoptotic cells, a process called efferocytosis, is impaired in atherosclerosis¹⁸, we reasoned that atorvastatin might increase the efferocytosis rate and thus beneficially impact lesion development. To test this hypothesis, we first employed an *in vitro* phagocytosis assay using macrophages as phagocytes and target cells. We observed by flow cytometry a relevant increase of the efferocytic rate of apoptotic cells upon combined treatment (atorvastatin plus SHP1i) compared to single therapies (Figure 3a and Extended Data Figure 3a). Of note, Bliss independence model confirmed additivity (Figure 3b). As previously shown, inhibition of the CD47-SIRP α axis (using anti-CD47 antibodies¹¹ or SHP1i¹³) did not alter the rate of programmed cell death quantified by caspase 3/7 activity in our cells. Similarly, we did not find an effect on apoptosis by atorvastatin or combined treatment strategies (Figure 3c and Extended Data Figure 3b), suggesting an enhancement of efferocytosis without altering apoptosis.

To determine the relevance of these observations *in vivo*, we also investigated the cleaved caspase-3 activity and the number of 'free' apoptotic bodies not associated with an intraplaque macrophage, both reliable measures of accumulation of apoptotic bodies and thus efferocytosis in tissue specimens. In agreement with our *in vitro* observations, we found a decrease in the number of apoptotic bodies in the lesion with the combined treatment, as suggested by our immunofluorescence studies (Figure 3d – 3e and Extended Data Figure 3c – 3d). Again, Bliss independence model demonstrated additivity (Figure 3f). Taken together, these data suggested that the combination of HMG-CoA reductase inhibition and

CD47-SIRP α blockade markedly increased the efferocytosis rate and thus may explain the additive effect on atherosclerotic plaque activity.

Atorvastatin directly regulated gene expression of Cd47

Having identified the efferocytic rate as a pivotal link for additivity of combined treatment, we sought to elucidate the underlying mechanism. Given the critical emerging role of the key 'don't-eat-me' molecule CD47 in atherosclerosis and efferocytosis, we hypothesized that there might be a direct effect of atorvastatin on CD47 expression. To answer this question, we investigated the Cd47 expression in two of the major cellular components of atherosclerosis, smooth muscle cells and macrophages. Stimulation with tumor necrosis factor- α increased Cd47 expression, but interestingly this effect was more pronounced in smooth muscle cells compared to macrophages. Consequently, treatment with atorvastatin resulted in a larger reduction of Cd47 on both RNA and protein levels in smooth muscle cells (Figure 4a – 4d and Extended Data Figure 4a – 4c).

To directly link atorvastatin treatment with Cd47 expression in smooth muscle cells, we used a dual luciferase reporter assay, which quantified the relative change to basal values obtained from control-transfected cells. We observed that atorvastatin was able to inhibit the tumor necrosis factor- α induced Cd47 promoter activity (Figure 4e). Based on our previous studies¹¹, we hypothesized that this treatment might reduce the nuclear translocation of NF κ B1 p50, which is a known key transcriptional factor for CD47. In alignment with this hypothesis, we found that atorvastatin inhibited the nuclear translocation of NF κ B1 p50. Importantly, the effect was eliminated with the addition of mevalonate, an antagonist to atorvastatin (Figure 4f – 4g and Extended Data Figure 4d). While additional causation studies are warranted, these results suggested that atorvastatin directly reduced the pathological CD47 upregulation in atherosclerosis via inhibition of the pro-inflammatory factor NF κ B1 p50. These results may provide a mechanistic understanding for statin's pleiotropic benefits through their regulation of efferocytosis.

Human atherosclerosis

To determine if HMG-CoA reductase inhibitors result in lower CD47 expression during human atherogenesis, we evaluated carotid endarterectomy samples from the Munich Vascular Biobank. Of note, we found that patients receiving statin treatment had lower CD47 expression than a propensity score (age-, gender-, medication-, symptom-, and physical status-) matched cohort without such a medication (Figure 4h). While the potential for residual confounding exists, these data suggested that HMG-CoA reductase inhibitors reduce the pathological upregulation of CD47 in human atherosclerosis and thus may have additive effects on the efferocytosis rate upon combined treatment (Figure 5).

Discussion

The studies presented above provide new insights which may help explain the pleiotropic effects of statins. Here we show that statins augment efferocytosis by inhibiting the nuclear translocation of NF κ B1 p50 and suppressing expression of the key 'don't eat me' molecule CD47. We demonstrate that statins amplify the anti-atherosclerotic effects of two recently

described pro-efferocytic therapies, and do so independent of any lipid-lowering effect. Analyses of clinical biobank specimens suggest a similar link between statins and CD47 expression in humans, highlighting the potential translational implications of these findings. Together, these results provide a possible mechanism for how statins provide benefit beyond their well-described effect on cholesterol metabolism, highlighting the possibility that they may also reduce atherosclerosis by exerting a pro-phagocytic and anti-inflammatory effect directly in the vessel wall.

For decades, researchers have had difficulty attributing the outsized clinical benefit associated with statins solely to their impact on low-density lipoprotein levels. For example, patients randomized to intensive statin therapy on hospital admission for an acute coronary syndrome experience a reduction in clinical event rates in the first 16 weeks (MIRACL study)¹⁹ or as early as 30 days after the start of therapy (PROVE IT-TIMI 22)²⁰. This early time-benefit window may be ascribed to a wide range of potential anti-inflammatory mechanisms, including reduced C-reactive protein⁶, T cell activation and endothelial function modulation via Krüppel-like factor 2^{21,22}, leukocyte-endothelial cell adhesion²³, and/or inhibition of prenylation of small G proteins^{24,25}. The fact that atorvastatin restores dysfunctional efferocytosis in atherosclerosis is therefore interesting, given that efferocytosis signalling is thought to occur independently of traditional risk factors, and has been directly linked to inflammation downstream of tumor necrosis factor- α ¹¹. As evidence continues to accrue showing that anti-cytokine agents such as canakinumab (interleukin-1 β , CANTOS)⁹ and ziltivekimab (interleukin-6, RESCUE)²⁶ may be promising targets in cardiovascular disease, it is tempting to speculate whether the disproportionately powerful effects of statins on atherosclerosis may be mediated, in part, via the clearance of inflammatory cells within the necrotic core.

While prior studies have suggested that statins can increase the rate of phagocytosis, the mechanism has been elusive to date^{27,28}. Here we demonstrate that atorvastatin is directly linked to the critical ‘don’t eat me’ molecule CD47 and thus to the removal of apoptotic debris, supporting a causal relationship. Signalling studies have demonstrated that statins inhibit the nuclear translocation of the inflammatory transcription factor NF κ B1 p50 in vascular cells^{7,29}. Because statins are being repurposed for use in other systemic inflammatory disorders, such as rheumatoid arthritis, inflammatory bowel disease, and systemic lupus erythematosus^{30–32}, it is interesting to speculate that any benefit they might provide could be primarily mediated through effects on the TNF- α -CD47 axis, given that these are lipid-independent diseases.

New therapeutic options are urgently needed in cardiovascular medicine. The finding that pro-efferocytic therapies amplify the pleiotropic benefits of statins in mice is therefore interesting, particularly given our translational observation that statin usage is associated with lower vascular CD47 expression in humans. It is also important to note that this observed benefit occurs independent of classical risk factors like hypertension, glucose, and lipid levels, which is consistent with prior reports studying these agents in vascular models^{11,13,33–35}. Because pro-phagocytic therapies reduce risk irrespective of traditional risk pathways (which can already be addressed with currently-available medicines), we hypothesize that reactivating intraplaque efferocytosis is an auspicious target for the

residual inflammatory risk in atherosclerosis. Our approach involves targeting either CD47 or SIRP α 's downstream effector molecule, SHP-1. Although we have recently provided the first evidence that an anti-CD47 antibody may reduce vascular inflammation in humans¹⁴, additional dose-ranging studies are needed to address the expected transient anaemia induced by anti-CD47 therapy³⁶. Given the observed additive effect of dual treatment, we anticipate that combination therapy with lower doses of anti-CD47 antibodies might maintain full efficacy, while hopefully providing a method to avoid induction of erythrophagocytosis. While CD47 is ubiquitously expressed (including on red blood cells), its receptor, SIRP α , is largely restricted to myeloid cells, such as macrophages in the atherosclerotic plaque. For this reason, the benefit observed after blockade of SIRP α 's downstream signalling molecule, SHP-1, provides proof-of-concept for more precise targeting of this axis, and could spur future clinical investigations on anti-SIRP α antibodies that theoretically should also have few, if any, off-target toxicities. Finally, it is worth noting that statins have much more potent lipid-lowering effects in humans than in mice^{33–35}. Accordingly, it is tempting to speculate whether the *additive* benefits of combination therapy observed in the current preclinical study may actually become *synergistic* when advanced to clinical trials, where concomitant LDL reduction can be expected.

In conclusion, our data show that atorvastatin promotes efferocytosis via a reduction in CD47, leading to a lipid-independent anti-atherosclerotic effect. Additionally, the combination of CD47-SIRP α blockade and HMG-CoA reductase inhibition amplifies the phagocytic capacity of macrophages and thus prevents necrotic core expansion in an additive manner. An important area of future research will be to understand which target, CD47 or SIRP α , is the most suitable in humans and which provides the most favourable therapeutic window. If successful, pro-efferocytic strategies could become a new orthogonal therapy on top of guideline-directed medications to further reduce the complications of atherosclerotic vascular disease.

Methods

Preparation of single-walled carbon nanotubes

Single-walled carbon nanotubes were prepared as previously reported¹³. Briefly, raw high-pressure catalytic decomposition of carbon nanotubes (diameter 0.8–1.2 nm, Unidym) were added in an aqueous solution of 1,2-distearoyl-sn-glycero-3-phosphoethanolamine-polyethylene glycol₅₀₀₀-amine (DSPE-PEG, Nanosoft Polymers, Catalogue# 2828–5000), sonicated for at least 1 hour and then centrifuged at 100,000 g for 1 hour to obtain PEGylated single-walled carbon nanotubes. Unbound surfactant was washed by repeated filtration through 100 kDa filters (Millipore Sigma, Catalogue# UFC910024). For conjugation of Cy5.5 Mono NHS Ester (GE Healthcare, Catalogue# GEPA15601), Cy5.5 Mono NHS Ester was incubated with PEGylated single-walled carbon nanotubes solution (10:1 mole ratio) for 2 hours. Excess Cy5.5 dye was removed by five to six rounds of centrifugal filtration until the filtrate became clear (PEGylated single-walled carbon nanotubes loaded with fluorescent Cy5.5 probes are referred to hereafter as SWNT). SWNT concentrations were determined spectrophotometrically with an extinction coefficient of $7.9E6 \text{ M}^{-1}\cdot\text{cm}^{-1}$ at 808 nm. The small-molecule inhibitor NSC-87877 (Sigma-Aldrich,

Catalogue# NSC-87877) of SIRP α 's downstream effector molecule Src homology 2 domain-containing phosphatase-1 (SHP-1) was added to stirred SWNT at 4 °C (pH 7.4) overnight to form PEGylated single-walled carbon nanotubes loaded with fluorescent Cy5.5 probe and the small-molecule inhibitor (this system is referred to hereafter as SHP1i). After 24 hours of stirring, SHP1i was dialysed for another 24 hours next to PBS to remove unbound NSC-87877 molecules. The concentration of the loaded small-molecule inhibitor NSC-87877 was measured using a NanoDrop One (Thermo Scientific) at its absorption of 320 nm.

Bone marrow-derived macrophages and RNA sequencing

Bone marrow cells were isolated from male C57BL/6J mice (The Jackson Laboratory) at the age of 6–8 weeks and differentiated ex vivo to macrophages in DMEM supplemented with 10 % heat-inactivated foetal bovine serum (FBS), 100 U/ml penicillin and 100 μ g/ml streptomycin (HyClone GE HealthCare, SV30010), and 10 ng/ml murine M-CSF (PeproTech, Catalogue# 315–02, Lot# 0518245) for 7 to 10 days. After washing cells with pre-warmed PBS to remove non-attached cells, the attached primary mouse macrophages were incubated with 100 pM SWNT or SHP1i for 24 hours in serum-free medium at 37 °C. After collecting and washing cells twice with 2 % FBS-PBS, macrophages were sorted using a FACSAria cell sorter equipped with FACSDiva v6 software (BD Life Sciences, Stanford Shared FACS Facility). Channel compensations were performed using single-stained UltraComp eBeads (Thermo Scientific, Catalogue# 01–2222-41) or control macrophages. In addition, macrophages were stained with SYTOX Blue (Invitrogen, Catalogue# S34837) to discriminate and exclude non-viable cells. Viable cells (SYTOX Blue negative) were sorted with a 100 μ m nozzle into populations that were Cy5.5-positive and Cy5.5-negative and collected in 2 % FBS-PBS. Then RNA was extracted using the miRNeasy Mini Kit (Qiagen, Catalogue# 217004). In each group (SWNT and SHP1i), three biological replicates were sequenced. The RNA samples were sent to Novogene Co. (Sacramento, CA, USA) for sample quality control, library preparation, and sequencing. All samples passed quality control. Subsequently, cDNA library construction and sequencing were performed for each sample on an Illumina Novaseq 6000 platform with paired-end 150 bp reads. The data quality report is provided in Source Data Figure 1a. The sequencing data were uploaded to the Galaxy web platform, and we used the public server at usegalaxy.org to further analyse the data (version 2.0.1)³⁷. Briefly, quality control of sequencing data was performed using FastQC (v0.11.8). HISAT2 (v2.1.0) was used to map the reads to the reference genome (built-in mm10). FeatureCounts was then used to count the number of reads mapped, and DESeq2 (v1.22.1) was used to generate the list of differentially regulated genes. P values were adjusted for multiple testing using Benjamin-Hochberg false discovery rate. Pathway and upstream regulator analyses were performed using Ingenuity Pathway Analysis (IPA, Qiagen). Of note, the overlap p value in Figure 1b and Extended Data Table 2 measures whether there is an overlap between the dataset genes generated by the RNA sequencing and the genes that are regulated by statins (analysed by Fisher's Exact Test, IPA).

Animals and diet

All mice were housed in a pathogen-free animal facility and maintained on a 12-hour light:dark cycle at 22 °C with free access to food and water. Mice were acclimatized for 1–2 weeks before experiments. A total of 100 male apolipoprotein E-deficient (ApoE^{-/-}) mice (B6.129P2-Apoetm1Unc/J, 002052) on a C56BL/6J background (The Jackson Laboratory) at the age of 8 weeks were used for this study. The animals were assigned to the experimental groups by complete randomisation. For *a priori* power analysis, the following parameters were used based on prior experience with the therapeutic agents^{11–13}: α of 0.05; power of 0.80; expected attrition of 10 %; and effect size of 1.5 for atorvastatin and 1.2 for anti-CD47 antibodies and SHPi. 10 animals were allocated to the PBS and atorvastatin groups as well as at least 13 animals were allocated to the IgG, anti-CD47, anti-CD47 plus atorvastatin, SWNT, SHPi, and SHPi plus atorvastatin cohorts. 4 animals were not included in the results: 2 animals were euthanized due to skin lesions; 2 animals were excluded owing to poor quality of histopathology. Consequently, 9 animals in the PBS group, 10 animals in the atorvastatin group, 13 animals in the IgG group, 13 animals in the anti-CD47 group, 13 animals in the anti-CD47 plus atorvastatin group, 12 animals in the SWNT group, 11 animals in the SHPi group, and 15 animals in the SHPi plus atorvastatin group were finally analysed. Of note, lesion area of SHPi animals compared to SWNT treated animals were published in our previous analysis¹³. After 2 weeks on high-fat diet (21 % anhydrous milk fat, 19 % casein, and 0.15 % cholesterol, Catalogue# 101511, Dyets Inc.), the indicated treatment was initiated and continued for the ensuing 9 weeks: (1) PBS by daily gavage versus atorvastatin (Lipitor, Pfizer, prescription formulation) at a dose of 10 mg/kg body weight per day by daily gavage¹²; (2) 200 μ g of the inhibitory anti-CD47 antibody (BioXCell, MIAP410, Catalogue# BE0283, Lot# 705318N1) IP every other day versus 200 μ g of the IgG1 isotype control (BioXCell, MOPC-21, Catalogue# BE0083, Lot# 619916O1B) IP every other day¹¹; or (3) SWNT at a dose of 200 μ l of 400 nM IV once-weekly versus SHPi at a dose of 200 μ l of 400 nM IV once-weekly¹³. Animal studies were approved by the Stanford University Administrative Panel on Laboratory Animal Care (protocol# 27279) and conformed to the NIH guidelines for the care and use of laboratory animals.

Tissue preparation and histological analyses

Tissue preparation and histological analyses were performed as previously described^{11,12}. After blood sample collection, mice were perfused with PBS via cardiac puncture and then perfusion fixed with 4 % phosphate-buffered paraformaldehyde. Blood samples were analysed by the Stanford Animal Diagnostic Laboratory. The entire aortic arch was carefully collected, embedded in optimal cutting temperature compound (VWR, Catalogue# 25608–930), and sectioned using a cryostat (Leica CM 1950). A total of six sections at 70 μ m distance from the base of the aortic root were collected and analysed from each mouse. Plaque area (in mm² and % of total vessel area) was quantified by Oil-red O staining (Sigma-Aldrich, Catalogue# O1516) and determined from the luminal aspect of the blood vessel through the plaque to the internal elastic lamina. Total vessel area was calculated by encircling the external elastic lamina. Necrotic core (in mm² and % of lesion area) was quantified by Masson's trichrome staining (Richard-Allen Scientific, Catalogue# 22–110-648) and defined as the neointimal area devoid of cellular tissue. Owing

to the insensitivity to angles at sectioning³⁸, fraction area (and not absolute surface) was chosen for result presentation in Figure 2. However, all results are reported and presented in Extended Data Figure 2. For immunofluorescence staining of atherosclerotic lesions, cryosections were blocked using 5 % goat serum (Sigma-Aldrich, Catalogue# G9023) in PBS. Next, sections were incubated overnight at 4 °C with the following primary antibodies: Mac3 (BD Life Sciences, Catalogue# 550292, 1:100) and cleaved caspase-3 (Cell Signaling Technology, Catalogue# 9661, 1:200). After extensive washing, sections were incubated with secondary antibodies from Thermo Scientific: Alexa Fluor 647 goat anti-rat (Catalogue# A-21247, Lot# 2119156, 1:250) and Alexa Fluor 488 goat anti-rabbit (Catalogue# A11034, Lot# 2110499, 1:250). Counterstaining to visualize nuclei was performed by incubating with DAPI (4',6-diamidino-2-phenylindole). Histological sections were imaged using a Zeiss Axioplan (equipped with a Nikon camera) or Leica DMI8 microscope (equipped with a Leica DMC4500 colour camera). Fluorescence sections were imaged using a Leica DMI8 microscope (equipped with a Leica K5 camera). Sections were analysed using Image J/FIJI software (Version: 2.0.0/1.52p, NIH) in a blinded fashion.

Bliss independence model

The Bliss independence model is a well-established method to determine additivity/synergy of compounds. Of note, additivity means that two drugs equal the sum of parts, whereas synergy means that two drugs are greater than the sum of parts. The formula $E_c = E_a + E_b - E_a \cdot E_b$, where E_c is the combined effect produced by the combination of compounds a and b , describes how a combination of compounds should act if 'Bliss additivity' exists¹⁷. To explore the data, we randomly shuffled the results of the single treatment groups using GraphPad random list generator. Then, we calculated E_c for each pair (referred to hereafter as $E_{calculated}$) and compared these results to the observed results in the combined-treated cohort (referred to hereafter as $E_{observed}$). A non-significant p value was considered to denote additivity.

Cell culture

Primary bone marrow-derived macrophages were grown in DMEM growth medium (Thermo Scientific, Catalogue# 11995-065) supplemented with 10 % heat-inactivated foetal bovine serum (Thermo Scientific, Catalogue# SH3007103HI), 100 U/ml penicillin, and 100 µg/ml streptomycin (HyClone GE HealthCare, Catalogue# SV30010). Mouse aortic vascular smooth muscle cells (Cell Biologics, Catalogue# C57-6080, Lot# M120919W12) were cultured and maintained according to the manufacturer's instructions. All cells were cultured in a humidified 5 % CO₂ incubator at 37 °C. The cells were authenticated and tested for bacteria, yeast, fungi, and mycoplasma contamination by the supplier. Additionally, samples from vascular smooth muscle cells, bone marrow-derived macrophages, and RAW 264.7 macrophages were collected to rule out mycoplasma contamination by polymerase chain reaction (SouthernBiotech, Catalogue# 13100-01, Extended Data Figure 1d) and/or biochemical detection (Lonza, Catalogue# LT07-118 and LT07-518, Extended Data Figure 1e). 5 µl of the polymerase chain reaction product was mixed with bromophenol blue loading buffer and separated in a 1.5 % DNA gel electrophoresis using the GeneRuler 1 kb DNA Ladder (Thermo Scientific, Catalogue# SM0313). The following stimuli were applied to the cells in the experiments described below: atorvastatin (Sigma-Aldrich,

Catalogue# PZ001, Source#0000040035, Batch#0000079529), Dimethyl sulfoxide (DMSO, sterile, Sigma-Aldrich, Catalogue# D2650), recombinant mouse tumor necrosis factor- α (TNF- α , aa 80–235, R&D systems, Catalogue# 410-MT, Lot# CS1419081), DL-mevalonic acid 5-phosphate (Sigma-Aldrich, Catalogue# 79849, Lot# BCBT1529), staurosporine (Sigma-Aldrich, Catalogue# S4400), anti-CD47 antibody (BioXCell, MIAP410, Catalogue# BE0283, Lot# 792420D1), and IgG1 control (BioXCell, MOPC-21, Catalogue# BE0083, Lot# 722919A2). When atorvastatin was used, equal concentrations of DMSO was added to all respective controls. Of note, the final concentration (v/v) of DMSO was equal or less than 0.1 % to avoid toxic effects.

***In vitro* phagocytosis assay**

Standard *in vitro* phagocytosis assays were performed using RAW 264.7 macrophages as phagocytes and target cells. Phagocytes were treated with 10 μ M atorvastatin, 4 nM SHP1i, and equal concentrations of their respective controls (DMSO, SWNT) for 24 hours (in detail: ‘vehicle’ = SWNT + DMSO; ‘Statin’ = SWNT + atorvastatin; ‘SHP1i’ = SHP1i + DMSO; ‘SHP1i + Statin’ = SHP1i + atorvastatin). Apoptosis in target cells was induced by 1 μ M staurosporine for 4 hours at 37 °C. Target cells were labelled with 1.25 μ M CellTracker Orange CMRA Dye (Thermo Scientific, Catalogue# C34551) or 0.1 μ M CellTracker Green CMFDA Dye (Thermo Scientific, Catalogue# C2925) according to the manufacturer’s instructions. Phagocytes were detected by Cy5.5 or 0.3 μ M CellTracker Deep Red Dye (Thermo Scientific, Catalogue# C34565). Phagocytes and target cells were then co-cultured for 2 hours at 37 °C. Double positive cells (phagocytes = Cy5.5 or Deep Red-positive, target cells = Orange or Green-positive) were quantified using the LSRII equipped with FACSDiva v6 software (BD Life Sciences, Stanford Shared FACS Facility) and analysed by FlowJo10.7.1 (BD Life Sciences). Efferocytosis rate was defined as Q2 (double positive cells) divided by the sum of Q1 and Q2 (total number of apoptotic cells).

Apoptosis assay

The apoptosis assay was performed as previously described¹¹. To evaluate apoptosis, the luminometric Caspase-Glo 3/7 Assay System (Promega, Catalogue# G8091) was performed on cultured murine RAW 264.7 macrophages, according to the manufacturer’s protocol. Cells were seeded in 96-well plates at the density of 10,000 cells per well, grown at 37 °C and serum-starved for 24 hours. Apoptosis was induced with 1 μ M STS treatment for 4 hours in the presence or absence of 10 μ M atorvastatin, 4 nM SHP1i, or equal concentrations of their respective controls (DMSO, SWNT). For quantification, an iD3 luminometer (Molecular Devices) was used.

RNA isolation and quantitative polymerase chain reaction

To measure Cd47 expression, mouse smooth muscle cells and murine bone marrow-derived macrophages were exposed to DMSO, 10 μ M atorvastatin, 50 ng/ml TNF- α + DMSO, or 50 ng/ml TNF- α + 10 μ M atorvastatin for 48 hours. To measure Apoe, Gpx3, Rbl1, Rhob, and Xiap expression, bone marrow-derived macrophages were exposed to DMSO or 10 μ M atorvastatin for 48 hours. RNA was extracted from cell lysates using the miRNeasy Mini Kit (Qiagen, Catalogue# 217004) according to the manufacturer’s protocol or the TRIzol method (Invitrogen, Catalogue# 15596026). Then, RNA was quantified with a

NanoDrop One (Thermo Scientific). RNA was reverse transcribed using the High-Capacity RNA-to-cDNA Synthesis Kit (Applied Biosystems, Catalogue# 4387406). Quantitative polymerase chain reaction (PCR) of the cDNA samples was performed on a ViiA7 Real-Time PCR system or a QuantStudio 5 (both Applied Biosystems). Gene expression levels were measured using TaqMan Universal Master Mix II (Applied Biosystems, Catalogue# 4440047, Lot# 00762728) and commercially available TaqMan primers (Applied Biosystems). Data were quantified with the 2^{-Ct} method and normalized to Gapdh as an internal control. The following TaqMan Primers were used: Cd47 (Mm00495011_m1), Apoe (Mm01307193_g1), Gpx3 (Mm00492427_m1), Rbl1 (Mm01250721_m1), Rhob (Mm00455902_m1), Xiap (Mm01311594_mH), and Gapdh (Mm99999915_g1).

Flow cytometry

To measure Cd47 expression, mouse smooth muscle cells and bone marrow-derived macrophages were exposed to DMSO, 50 ng/ml TNF- α + DMSO, or 50 ng/ml TNF- α + 10 μ M atorvastatin for 48 hours. Cells were washed, harvested, and stained with an anti-CD47 antibody (BD Life Sciences, Catalogue# 561890, FITC, MIAP301, 0.5 mg/ml) or an isotype control antibody (BD Life Sciences, Catalogue# 553929, FITC, R35-95, 0.5 mg/ml) after Fc receptor blockade (BD Biosciences, Catalogue# 553142, anti-mouse CD16/CD32). Expression was quantified using the LSRII equipped with FACSDiva v6 software (BD Life Sciences, Stanford Shared FACS Facility) and analysed by FlowJo10.7.1 (BD Life Sciences). The ratio of fluorescence intensity (RFI) was calculated by dividing the median fluorescence intensity of CD47 by the median fluorescence intensity of IgG isotype control.

In vitro immunofluorescence

Mouse smooth muscle cells were seeded in Millicell EZ Slides (Sigma-Aldrich, Catalogue# PEZGS0416 or Catalogue# PEZGS0816). For CD47 staining, cells were exposed to DMSO, 50 ng/ml TNF- α + DMSO, or 50 ng/ml TNF- α + 10 μ M atorvastatin for 48 hours. For NF κ B1 p105/p50 staining, cells were first treated with DMSO, 10 μ M atorvastatin, or 10 μ M atorvastatin + 100 μ M mevalonate for 24 hours and then exposed to 50 ng/ml TNF- α for 45 minutes. Following stimulation/treatment, cells were rinsed with PBS and fixed with 4 % phosphate-buffered paraformaldehyde. For CD47 staining (BioXCell, MIAP410, 25 μ g/ml), vector mouse-on-mouse fluorescein Immunodetection Kit (Thermo Scientific, Catalogue# NC9801950) was used according to the manufacturer's instructions. For NF κ B1 p105/p50 staining, cells were blocked with 5 % goat serum (Sigma-Aldrich, Catalogue# G9023) for 30 minutes, then incubated with NF κ B1 p105/p50 (Cell Signaling Technology, Catalogue# 13586S, D4P4D, 1:200) overnight at 4 °C. After extensive washing, cells were incubated with Alexa Fluor 594 goat anti-mouse (Thermo Scientific, Catalogue# A-11005, Lot# 1696463, 1:300) or Alexa Fluor 647 goat anti-rabbit (Thermo Scientific, Catalogue# A-21244, Lot# 56897A, 1:300), and DAPI (4',6-diamidino-2-phenylindole). Images were captured using a Leica DMI8 microscope (equipped with a Leica DMC4500 colour camera and a Leica K5 camera for fluorescence imaging).

Luciferase reporter assay

The luciferase reporter assay was performed as previously described¹¹. CD47 LightSwitch Promoter Reporter GoClones (RenSP, S710450) and Cypridina TK Control constructs (pTK-

Cluc, SN0322S) were obtained from SwitchGear Genomics. 45 ng of the RenSP reporter and 5 ng of the pTK-Cluc reporter construct were transfected into mouse smooth muscle cells using Lipofectamine 3000 Transfection Reagent (Thermo Scientific, Catalogue# L3000-008) and Opti-MEM I Reduced Serum Medium (Thermo Scientific, Catalogue# 31985062). After 48 hours, media was changed to fresh medium and cells were then exposed to DMSO, 50 ng/ml TNF- α + DMSO, or 50 ng/ml TNF- α + 10 μ M atorvastatin. The cell lysate and supernatant were harvested 24 hours after stimulation/treatment and dual luciferase activity was measured with the LightSwitch Luciferase Assay Kit (Active Motif, Catalogue# 32031, NC0999256) and Pierce Cypridina Luciferase Glow Assay Kit (Thermo Scientific, PI16170) using an iD3 luminometer (Molecular Devices). Relative luciferase activity (RenSP/Cypridina ratio) was quantified as the percentage change relative to the basal value obtained from control-transfected cells.

Protein extraction and western blotting

To measure NF κ B1 p50 nuclear translocation, mouse smooth muscle cells were first treated with DMSO, 10 μ M atorvastatin, or 10 μ M atorvastatin + 100 μ M mevalonate for 24 hours and then exposed to 50 ng/ml TNF- α for 45 minutes. Total protein was isolated from mouse smooth muscle cells using a subcellular protein fractionation kit (Thermo Scientific, Catalogue# 78840) supplemented with Halt Protease and Phosphatase Inhibitor Cocktail (Thermo Scientific, Catalogue# 78442). The protein concentration in each sample was measured using Pierce BCA Protein Assay Kit (Thermo Scientific, Catalogue# 23225). Equal amounts of protein were loaded and separated on precast gels (Bio-Rad, Catalogue# 456-1084) and thereafter transferred onto PVDF membranes (Life Technologies, Catalogue# LC2002). Following 1 hour incubation in 5 % bovine serum albumin in 0.1 % TBS-T, these membranes were probed with commercially available antibodies designed to recognize NF κ B1 p105/p50 (Cell Signaling Technology, Catalogue# 13586S, D4P4D, 1:1000) and HDAC1 (Cell Signaling Technology, Catalogue# 5356S, 10E2, 1:1000) overnight at 4 °C. After extensive washing with 0.1 % TBS-T, membranes were incubated with secondary antibodies, Alexa Fluor 647 goat anti-mouse (Invitrogen, Catalogue# 32728, Lot# TA252659, 1:10,000) and Alexa Fluor 488 goat anti-rabbit (Thermo Scientific, Catalogue# A11034, Lot# 2110499, 1:10,000), for 1 hour. Membranes were then scanned with an iBright 1500 Imaging System (Thermo Scientific) for quantitative analysis using Image J/FIJI software (Version: 2.0.0/1.52p, NIH).

Human carotid artery tissue

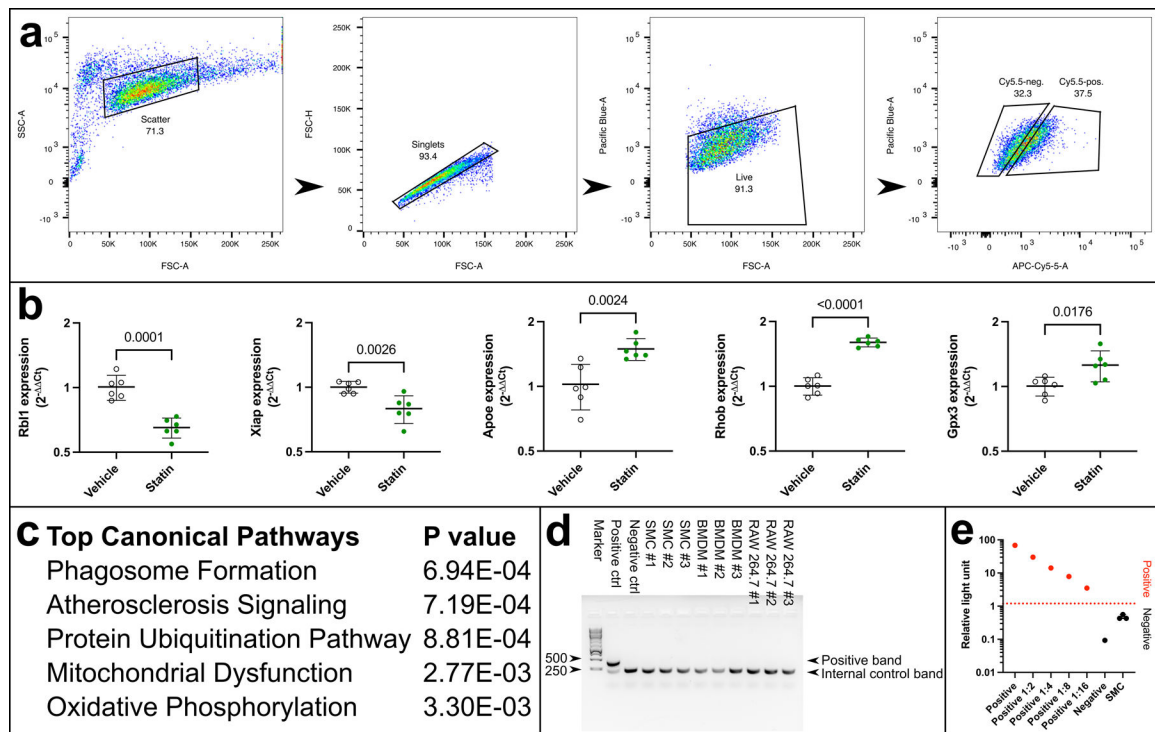
The Munich Vascular Biobank contains human atherosclerotic plaques and plasma samples, along with clinical data obtained from patients receiving carotid endarterectomy. The authors state that their study complies with the Declaration of Helsinki, that the locally appointed Institutional Review Board of the Technical University Munich (Germany) has approved the research protocol and that informed consent has been obtained from the subjects. In this study, a total of 14 human carotid endarterectomy samples were used as follows: age-, gender-, medication-, symptom-, and physical status-matched samples from 7 patients with statin medication were compared with 7 patients without such a medication (clinical data provided in Source Data Figure 4h). In an attempt to understand why these individuals were not treated with a statin, we reviewed each subject's clinical information.

We found that those individuals not on a statin were being seen by a vascular surgeon specialist for the first time and did not have other obvious contraindications to statin use such as liver failure or medical allergies which could have confounded the results. Nevertheless, patients who present for carotid endarterectomy are in general candidates for statin treatment and thus the 'No Statin' group may represent a skewed population. Of note, symptomatic stenosis was defined if the patient had suffered from carotid related symptoms, such as transient ischemic attack, amaurosis fugax (lasting < 24 hours), or stroke (defined as loss of neurological function lasting > 24 hours), within the last 6 months. Thus, our definition refers to clinical events and not a specific degree of stenosis. Carotid tissue was cut in approximately 50 mg pieces on dry ice. Homogenization of the tissue was performed in 700 μ l QIAzol lysis reagent and total RNA was isolated using the miRNeasy Mini Kit (Qiagen), according to the manufacturer's instruction. RNA concentration and purity were assessed using NanoDrop (Thermo Fisher Scientific). RNA integrity numbers for all samples were assessed using the RNA Screen Tape (Agilent) in the Agilent TapeStation 4200. Next, first strand cDNA synthesis was performed with the High-Capacity-RNA-to-cDNA Kit (Applied Biosystems), following the manufacturer's instruction. Gene expression levels were measured using commercially available TaqMan primers (Applied Biosystems), CD47 (Hs00179953_m1) and RPLP0 (Hs00420895_gH), on a QuantStudio 3 Cycler (Applied Biosystems) using 96 well plates.

Statistical analysis

Statistical analyses were performed using GraphPad Prism 9 (GraphPad Inc.). Mean \pm 95 % confidence interval was used for parametric results, median \pm interquartile range was used for non-parametric results. Approximately normally distributed data were analysed using an unpaired Student's *t*-test (two-tailed), a paired Student's *t*-test (two-tailed), a one-way analysis of variance with Tukey's or Sidak's multiple comparisons test, or a repeated measures analysis of variance with Tukey's multiple comparisons test. For data that were not approximately normally distributed, a Mann-Whitney *U* test (two-tailed) or a Kruskal-Wallis with Dunn's multiple comparisons test were used. Multiple comparisons tests were reported when the overall analysis of variance or Kruskal-Wallis test had a *p* value less than 0.05. All data behind the statistical analysis and all *p* values are provided in Source data. *P* values for the differentially expressed genes (Extended Data Table 1) were adjusted for multiple testing using Benjamin-Hochberg false discovery rate. Pathway and upstream regulator analyses (Figure 1b, Extended Data Figure 1c, and Extended Data Table 2) were performed using Ingenuity Pathway Analysis (IPA, Qiagen). The overlap *p* values were analysed by Fisher's Exact Test, calculated by IPA.

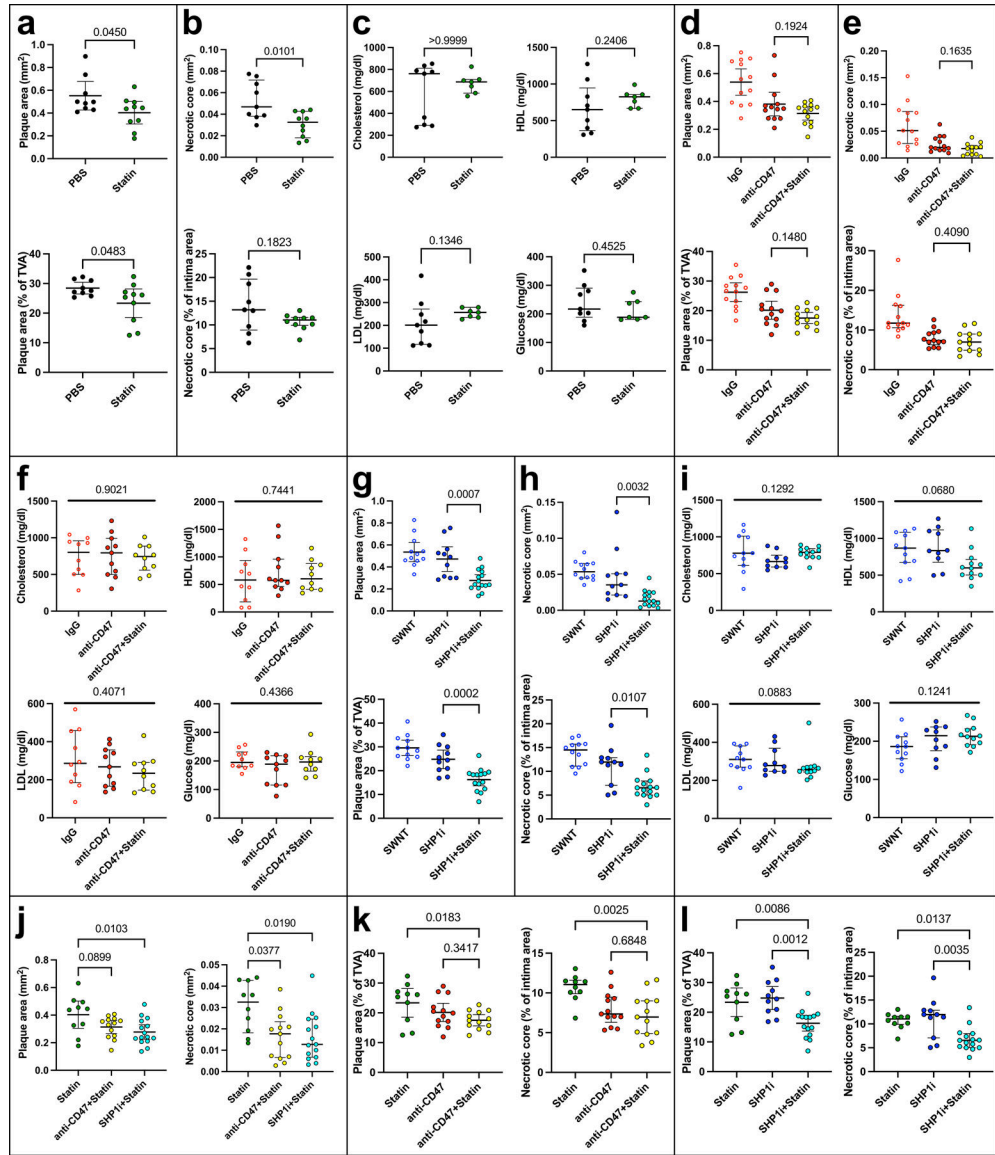
Extended Data



Extended Data Fig. 1: RNA sequencing revealed HMG-CoA reductase inhibitor as one of the top upstream regulators of SHP-1 inhibition in macrophages.

a, Flow cytometry gating strategy for cell sorting to isolate Cy5.5-positive bone marrow-derived macrophages in each group (SHP1i versus SWNT), which were then subjected to RNA sequencing. b, Rb1l1, Xiap, Apoe, Rhob, and Gpx3 expression by quantitative polymerase chain reaction in bone marrow-derived macrophages upon atorvastatin treatment (n = 6 biologically independent samples per group). c, Functional pathways enriched among all differential expressed genes (false-discovery rate < 0.10) as determined by pathway analysis (p-value of overlap). d – e, Samples from vascular smooth muscle cells, bone marrow-derived macrophages, and RAW 264.7 macrophages were collected to rule out mycoplasma contamination by polymerase chain reaction and/or biochemical detection (n = 3 biologically independent samples per group).

Each data point represents a biologically independent sample. Data and error bars present mean \pm 95 % confidence interval for parametric results. Data of (b) were analysed by unpaired Student's t-test (two-tailed). Data of (c) were analysed by Fisher's Exact Test, IPA.

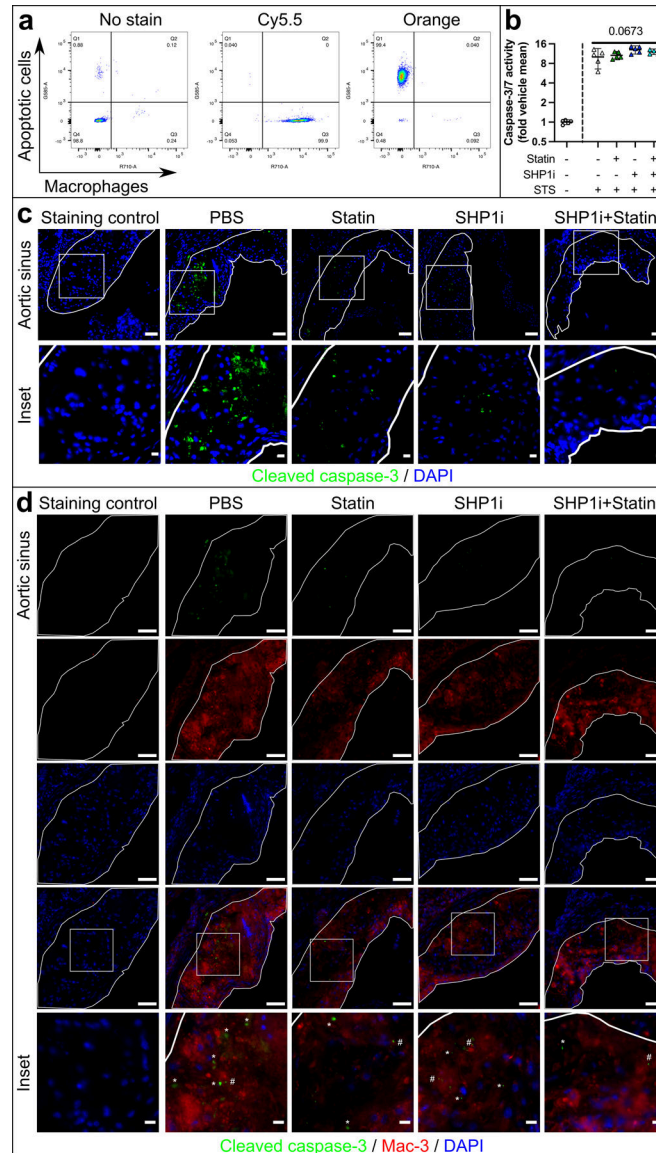


Extended Data Fig. 2: Combined treatment of CD47-SIRP α blockade and atorvastatin showed additive effects on atherosclerotic plaque activity in vivo.

a, Quantification of atherosclerotic lesion area (n = 9 for PBS; n = 10 for Statin). TVA, total vessel area. b, Quantification of necrotic core size (n = 9 for PBS; n = 10 for Statin). c, Quantification of total cholesterol, HDL, LDL, and glucose in the blood (n = 9 for PBS; n = 7 for Statin). d, Quantification of atherosclerotic lesion area (n = 13 for IgG; n = 13 for anti-CD47; n = 13 for anti-CD47+Statin). e, Quantification of necrotic core size (n = 13 for IgG; n = 13 for anti-CD47; n = 13 for anti-CD47+Statin). f, Quantification of total cholesterol, HDL, LDL, and glucose in the blood (n = 10 for IgG; n = 11 for anti-CD47; n = 10 for anti-CD47+Statin). g, Quantification of atherosclerotic lesion area (n = 12 for SWNT; n = 11 for SHP1i; n = 15 for SHP1i+Statin). h, Quantification of necrotic core size (n = 12 for SWNT; n = 11 for SHP1i; n = 15 for SHP1i+Statin). i, Quantification of total cholesterol, HDL, LDL, and glucose in the blood (n = 11 for SWNT; n = 10 for SHP1i; n = 12 for SHP1i+Statin). j – l, Quantification of atherosclerotic lesion area and necrotic core size (n =

10 for Statin; n = 13 for anti-CD47; n = 13 for anti-CD47+Statin; n = 11 for SHP1i; n = 15 for SHP1i+Statin).

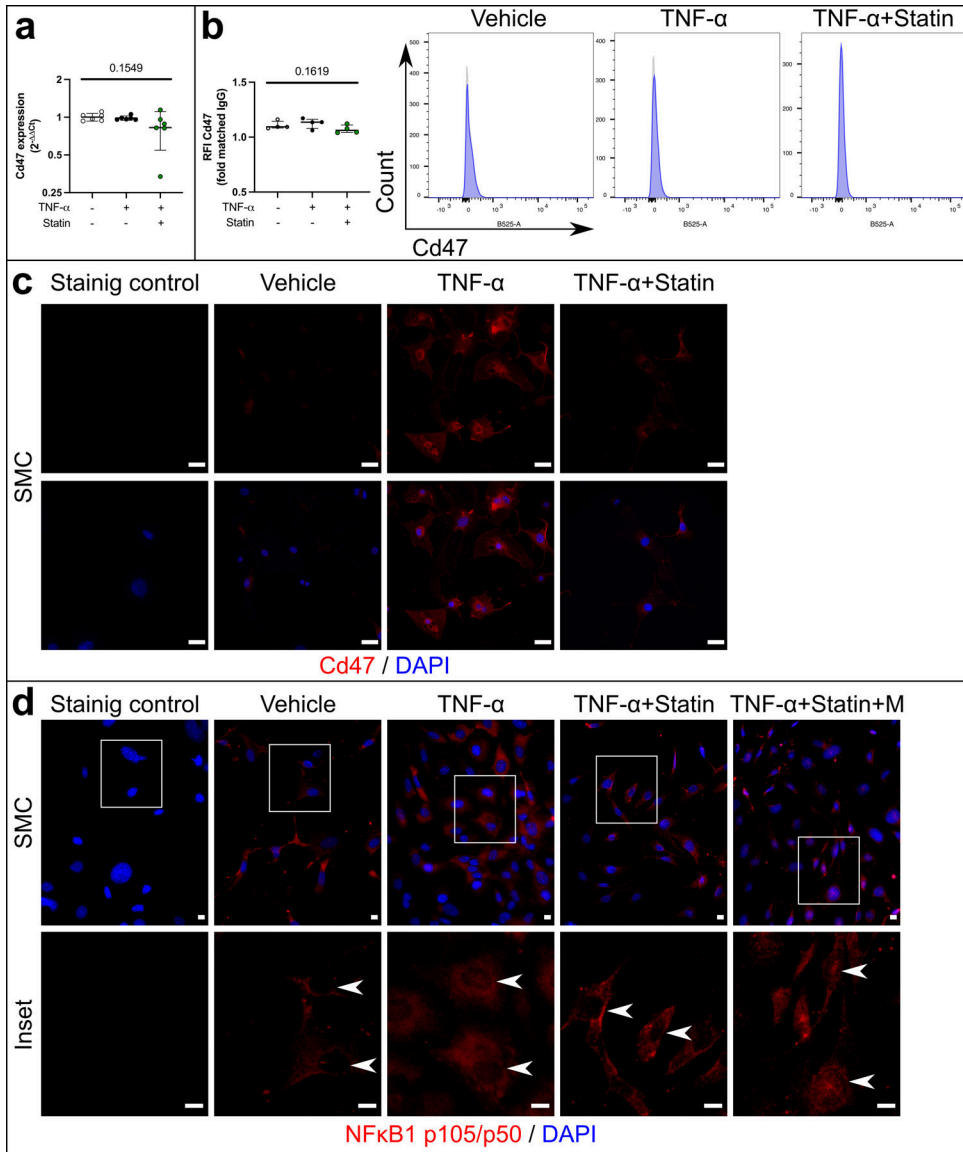
Each data point represents a biologically independent animal. Data and error bars present mean \pm 95 % confidence interval for parametric and median \pm interquartile range for non-parametric results. Data of (a) were analysed by unpaired Student's t-test (two-tailed). Data of (b - c) were analysed by Mann-Whitney U test (two-tailed). Data of (d), (g), and (j - l) were analysed by one-way analysis of variance with Sidak's multiple comparisons test. Data of (e - f) and (h - i) were analysed by Kruskal-Wallis with Dunn's multiple comparisons test.



Extended Data Fig. 3: Combined treatment of CD47-SIRP α blockade and atorvastatin showed additive effects on efferocytosis rate in vitro and in vivo.

a, Flow cytometry plots depicting the staining controls for the conditions. b, Apoptosis assay to quantify the rate of programmed cell death in vitro in the presence or absence

of atorvastatin, SHP1i, and dual treatment after staurosporine (STS) stimulation (n = 5 biologically independent samples per group). c, Immunofluorescence images depicting cleaved caspase-3 activity (n = 9 for PBS; n = 10 for Statin; n = 11 for SHP1i; n = 15 for SHP1i+Statin). White line depicts intima. Scale bar, 50 μ m; scale bar inset, 10 μ m. d, Immunofluorescence images depicting the ratio of free to macrophage associated cleaved caspase-3 activity (n = 9 for PBS; n = 10 for Statin; n = 11 for SHP1i; n = 15 for SHP1i+Statin). White line depicts intima. *, free cleaved caspase-3. #, macrophage-associated cleaved caspase-3. Scale bar, 50 μ m; scale bar inset, 10 μ m. Each data point represents a biologically independent sample. Data and error bars present mean \pm 95 % confidence interval for parametric results. Data of (b) were analysed by one-way analysis of variance test.



Extended Data Fig. 4: Atorvastatin inhibited NF κ B1 p50 nuclear translocation under atherogenic conditions and thus directly regulated gene expression of Cd47.

a, Cd47 expression by quantitative polymerase chain reaction in bone marrow-derived macrophages (n = 6 biologically independent samples per group). TNF- α , tumor necrosis factor- α . b, Cd47 expression by flow cytometry in bone marrow-derived macrophages (n = 4 biologically independent samples per group). RFI, ratio of median fluorescence intensity. c, Cd47 expression by immunofluorescence in smooth muscle cells (n = 10 cells for vehicle and n = 15 cells for TNF- α or TNF- α +Statin examined over 3 biologically independent samples per group). SMC, smooth muscle cells. Scale bar, 10 μ m. d, NF κ B1 p50 nuclear translocation by immunofluorescence in smooth muscle cells (n = 3 biologically independent samples per group). NF κ B1, nuclear factor of kappa light polypeptide gene enhancer in B cells 1. M, mevalonate. Scale bar and scale bar inset, 10 μ m. Each data point of represents a biologically independent sample. Data and error bars present mean \pm 95 % confidence interval for parametric and median \pm interquartile range for non-parametric results. Data of (a) were analysed by one-way analysis of variance test. Data of (b) were analysed by Kruskal-Wallis test.

Extended Data Table 1.

Differentially expressed genes that regulate the response to SHPI1 in bone marrow-derived macrophages.

DESeq2 result file, FDR<0.10.

Symbol	Base mean	log ₂ (FC)	StdErr	Wald-Stats	P-value	P-adjusted for multiple testing using Benjamin-Hochberg false discovery rate
Npm1	3242.05193	-0.682194	0.1174676	-5.807505	6.341E-09	5.968E-05
Nap1l1	2994.05004	-0.595259	0.114621	-5.193281	2.066E-07	0.0009724
Ccr2	371.946841	-0.894528	0.1793836	-4.986678	6.143E-07	0.0019271
ND5	20290.2329	-0.676315	0.1483706	-4.55828	5.157E-06	0.0121354
Xpo1	1219.2632	-0.693269	0.1561322	-4.440267	8.985E-06	0.0133478
Top2a	1545.38136	-0.649076	0.1494088	-4.344294	1.397E-05	0.0133478
Psmc6	478.627038	-0.746306	0.1703417	-4.381228	1.18E-05	0.0133478
Cbx5	835.971462	-0.718755	0.1645141	-4.368958	1.248E-05	0.0133478
Samd9l	709.663395	-0.776114	0.1787856	-4.341029	1.418E-05	0.0133478
ND1	17212.9014	-0.671797	0.1517261	-4.427694	9.525E-06	0.0133478
Cd36	36728.2051	-0.514444	0.1206735	-4.263109	2.016E-05	0.0172498
Ccl9	5541.05535	-0.588759	0.13967	-4.215357	2.494E-05	0.0180554
Rps6ka3	1342.56276	-0.596286	0.1414151	-4.21657	2.48E-05	0.0180554
Rnasek	2295.51587	0.4740923	0.1131065	4.1915568	2.77E-05	0.0181791
Mfge8	48853.4169	0.4938391	0.1181038	4.1813983	2.897E-05	0.0181791
Gm8995	1806.60392	-0.583836	0.1419539	-4.112855	3.908E-05	0.0229885
Rps24	4095.7711	-0.522726	0.1278387	-4.088949	4.333E-05	0.0239913
Cpne3	1392.2146	-0.549763	0.1350771	-4.069992	4.701E-05	0.0245835
Arfgef1	1634.00062	-0.530296	0.1314385	-4.034551	5.471E-05	0.025745
CYTB	19258.079	-0.612887	0.1516754	-4.040783	5.327E-05	0.025745
Arhgap5	453.486631	-0.694198	0.1745749	-3.976503	6.994E-05	0.0274266
Fam208b	361.7303	-0.676217	0.1691563	-3.99759	6.399E-05	0.0274266

DESeq2 result file, FDR<0.10.

Symbol	Base mean	log2(FC)	StdErr	Wald-Stats	P-value	P-adjusted for multiple testing using Benjamin-Hochberg false discovery rate
Matr3	1315.53676	-0.619373	0.1549832	-3.996386	6.432E-05	0.0274266
Fam111a	1284.34979	-0.666224	0.1675363	-3.976596	6.991E-05	0.0274266
Cd200r4	822.550513	-0.577772	0.1462751	-3.949897	7.818E-05	0.029435
Abcb7	1007.56014	-0.613717	0.1561756	-3.929656	8.507E-05	0.0307944
Rasa1	4026.78695	-0.474062	0.1217859	-3.892584	9.918E-05	0.0333394
mt-Rnr2	6366.19569	-0.572217	0.1469666	-3.893517	9.88E-05	0.0333394
Nufip2	1090.14958	-0.589902	0.1519558	-3.882062	0.0001036	0.0336152
Rpl5	6449.20695	-0.39906	0.1032139	-3.866341	0.0001105	0.0346614
Stag2	1753.1737	-0.583361	0.1527947	-3.81794	0.0001346	0.0408574
ND2	6807.98383	-0.580048	0.1529778	-3.791711	0.0001496	0.0440049
Rps26	8802.52273	0.3743714	0.100227	3.7352349	0.0001875	0.0464507
Polr2b	1005.07336	-0.518873	0.1385658	-3.744598	0.0001807	0.0464507
Capza2	2435.66898	-0.551051	0.1474399	-3.737459	0.0001859	0.0464507
Apoe	314459.196	0.4075395	0.1090798	3.7361598	0.0001869	0.0464507
ND6	4229.26473	-0.604856	0.1615997	-3.742929	0.0001819	0.0464507
Usp9x	2594.47463	-0.574506	0.1523877	-3.770028	0.0001632	0.0464507
Ipo7	1702.3695	-0.564834	0.1523259	-3.708063	0.0002089	0.0504027
Hvcn1	11357.9652	0.3982316	0.1076978	3.6976772	0.0002176	0.0504876
Ube3a	679.408836	-0.555129	0.1502401	-3.694949	0.0002199	0.0504876
Med13	1288.31486	-0.536446	0.146008	-3.674088	0.0002387	0.0534916
Pgap1	1849.06388	-0.529838	0.1447107	-3.661361	0.0002509	0.0537002
Tpm4	4564.90452	-0.427339	0.1167211	-3.661194	0.000251	0.0537002
Atp6v0d2	9161.22894	-0.390628	0.1070645	-3.648527	0.0002637	0.0539652
Slc12a9	1220.70435	0.4833671	0.1324721	3.6488221	0.0002634	0.0539652
Acer3	949.045824	-0.541325	0.1488204	-3.637438	0.0002754	0.0551429
Mad2l1	227.982466	-0.643762	0.1772805	-3.631317	0.000282	0.0552913
Chml	186.52479	-0.67047	0.1854697	-3.614982	0.0003004	0.0565413
Clec4a2	741.708363	-0.613202	0.1694017	-3.619812	0.0002948	0.0565413
Trip12	6228.35021	-0.399155	0.1111046	-3.592602	0.0003274	0.0604199
Rgs18	332.45645	-0.655479	0.1828842	-3.584123	0.0003382	0.0612166
Zfp715	367.852161	-0.615505	0.1726816	-3.564391	0.0003647	0.0635662
Taf1	976.459203	-0.511205	0.1433914	-3.565099	0.0003637	0.0635662
Sept2	4279.86171	-0.396537	0.1119631	-3.541675	0.0003976	0.0661757
Itgb5	22956.8691	0.351362	0.0992666	3.5395786	0.0004008	0.0661757
Zfp655	478.800926	-0.583368	0.1645507	-3.545216	0.0003923	0.0661757
Itsn2	2693.96828	-0.411825	0.1166974	-3.529	0.0004171	0.0665434
Ddx3y	590.76308	-0.607796	0.1720845	-3.531963	0.0004125	0.0665434
Itga4	3079.09814	-0.43504	0.1234488	-3.524054	0.000425	0.066668
9930021J03Rik	492.017401	-0.559776	0.1594563	-3.510531	0.0004472	0.0690027

DESeq2 result file, FDR<0.10.

Symbol	Base mean	log2(FC)	StdErr	Wald-Stats	P-value	P-adjusted for multiple testing using Benjamin-Hochberg false discovery rate
Ahctf1	994.321727	-0.462714	0.1321369	-3.501779	0.0004622	0.0690456
Fgd4	1521.70743	-0.466917	0.1332277	-3.504657	0.0004572	0.0690456
Evi5	614.023254	-0.537295	0.1541705	-3.485073	0.000492	0.0723552
Belaf1	1173.05171	-0.505358	0.1457404	-3.467519	0.0005253	0.0742996
Hsp90aa1	3232.39853	-0.442235	0.1277848	-3.460781	0.0005386	0.0742996
2010111I01Rik	1228.62748	0.4945969	0.1426575	3.4670226	0.0005263	0.0742996
Stap1	1595.34585	-0.466193	0.1348254	-3.457756	0.0005447	0.0742996
Msr1	3513.1522	-0.475334	0.1374617	-3.457937	0.0005443	0.0742996
Rhob	5872.50112	0.3708907	0.107636	3.4457885	0.0005694	0.076435
Scoc	202.246063	-0.650447	0.188952	-3.442393	0.0005766	0.076435
Tfrc	837.391924	-0.618628	0.1805568	-3.426223	0.000612	0.0768164
Copg2	768.705153	-0.572456	0.1670824	-3.426189	0.0006121	0.0768164
Tlr8	2373.17965	-0.562589	0.1640763	-3.428822	0.0006062	0.0768164
Tlr7	1571.66003	-0.571586	0.1665331	-3.432265	0.0005986	0.0768164
Rev3l	277.223427	-0.598769	0.1751333	-3.41893	0.0006287	0.0768457
Tmem86a	2239.55452	0.3995808	0.1168405	3.4198837	0.0006265	0.0768457
Stag1	774.722848	-0.484919	0.1421563	-3.411167	0.0006469	0.0780537
Zfp91	1358.06722	-0.505763	0.1486214	-3.403026	0.0006664	0.0793991
Washc4	1511.88813	-0.491068	0.144936	-3.38817	0.0007036	0.0807842
Plek	4443.47095	-0.424576	0.1255595	-3.381474	0.000721	0.0807842
Usp34	1261.85362	-0.579528	0.171077	-3.387527	0.0007053	0.0807842
Gmfb	1907.76758	-0.49446	0.145912	-3.388757	0.0007021	0.0807842
Sept7	1372.36512	-0.566735	0.1674484	-3.384537	0.000713	0.0807842
Rrm2b	200.05789	-0.611686	0.1813308	-3.373316	0.0007427	0.0809552
Rasgrp3	2117.6771	-0.413762	0.1227328	-3.371238	0.0007483	0.0809552
Csde1	4109.66547	-0.451253	0.1336798	-3.375628	0.0007365	0.0809552
Bmt2	1425.88128	-0.466013	0.1383796	-3.367641	0.0007581	0.0810867
Kcnj2	3953.7074	-0.435799	0.1299692	-3.353094	0.0007991	0.083208
Rbl1	604.266761	-0.520517	0.1552328	-3.353135	0.000799	0.083208
Ptbp3	4010.82917	-0.419232	0.1250976	-3.351243	0.0008045	0.083208
Sssca1	223.023386	0.5979708	0.1787979	3.3443954	0.0008246	0.0843623
Pds5a	1395.68393	-0.409586	0.1229404	-3.331579	0.0008635	0.0863621
Cnot7	425.652524	-0.590258	0.1771688	-3.331611	0.0008634	0.0863621
Dop1a	410.59511	-0.571328	0.1716235	-3.328964	0.0008717	0.0863621
Ccdc82	448.593532	-0.520161	0.1566159	-3.32125	0.0008962	0.0878601
Gpx3	1203.55945	0.5103464	0.1538418	3.3173468	0.0009088	0.0881786
Eeal	2176.65588	-0.421481	0.1276965	-3.300647	0.0009646	0.0908325
Cd44	7136.17639	-0.366927	0.1111777	-3.300363	0.0009656	0.0908325
Fnbp11	1203.25197	-0.51752	0.1570643	-3.294956	0.0009844	0.0908325

DESeq2 result file, FDR<0.10.

Symbol	Base mean	log2(FC)	StdErr	Wald-Stats	P-value	P-adjusted for multiple testing using Benjamin-Hochberg false discovery rate
Phip	1143.90535	-0.51337	0.1557288	-3.296561	0.0009788	0.0908325
Dock11	1274.14705	-0.526564	0.1596636	-3.29796	0.0009739	0.0908325
Xiap	1712.20606	-0.492271	0.1497678	-3.286899	0.001013	0.0925641
Prpf40a	1307.27288	-0.511801	0.1560702	-3.279299	0.0010407	0.0932609
Ola1	712.79889	-0.491614	0.1501495	-3.27416	0.0010598	0.0932609
Gm5148	123.970025	-0.616538	0.1883112	-3.274035	0.0010602	0.0932609
Htati2	854.624986	0.459485	0.1401437	3.2786696	0.001043	0.0932609
Acs13	422.228347	-0.564916	0.1730758	-3.26398	0.0010986	0.0948616
Cacul1	3093.84835	-0.366018	0.1121274	-3.264309	0.0010973	0.0948616
Opa1	1628.93838	-0.402782	0.1237286	-3.255371	0.0011324	0.0960229
Aldh2	18855.8723	0.3284566	0.1008356	3.2573458	0.0011246	0.0960229
Cd84	10383.0594	-0.40313	0.1246763	-3.233411	0.0012232	0.096935
Ranbp2	2516.39428	-0.476745	0.1473101	-3.236335	0.0012108	0.096935
Cstb	8504.67637	0.387462	0.1192154	3.2500993	0.0011536	0.096935
Ccdc88a	926.625389	-0.499509	0.1539842	-3.243895	0.0011791	0.096935
Dab2	5027.67442	-0.476548	0.1475169	-3.230465	0.0012359	0.096935
Brpf3	762.946765	0.4554884	0.14098	3.2308733	0.0012341	0.096935
Mul1	870.270732	0.4312835	0.133091	3.2405152	0.0011931	0.096935
Psd3	567.69153	-0.542798	0.1676655	-3.237383	0.0012063	0.096935
Myo9a	548.435199	-0.548281	0.1691602	-3.241196	0.0011903	0.096935
Tmem167	525.222078	-0.556529	0.1725718	-3.224915	0.0012601	0.0980171
Smc6	905.650771	-0.483238	0.1500667	-3.220156	0.0012812	0.0984595
Tef	2046.49037	0.4008578	0.1246214	3.2166049	0.0012972	0.0984595
Mfsd5	2335.47547	0.3597961	0.1118082	3.2179767	0.001291	0.0984595
Dnajb4	703.518491	-0.555447	0.1731111	-3.208616	0.0013338	0.0988675
Zfp644	353.391977	-0.565954	0.1763894	-3.20855	0.0013341	0.0988675
Far1	1085.41851	-0.502354	0.1563606	-3.212788	0.0013145	0.0988675
Cnot6l	761.651586	-0.513302	0.1602367	-3.203399	0.0013582	0.099867

Extended Data Table 2.

Upstream regulators predicted by Ingenuity Pathway Analysis.

Upstream regulator	Molecular type	Predicted state	Z-score	P value of overlap
Actinonin	Chemical reagent	Activated	2.236	3.23E-08
SIRT3	Enzyme	Activated	2.416	7.75E-07
Lovastatin	Chemical drug	Activated	2.184	1.55E-03
HNF4A	Transcription regulator	Activated	2.39	3.73E-02
DAP3	Other	Inhibited	-2.236	6.83E-09
LONP1	Peptidase	Inhibited	-2.236	7.84E-05

Upstream regulator	Molecular type	Predicted state	Z-score	P value of overlap
TFE3	Transcription regulator	Inhibited	-2	1.48E-04
IL6	Cytokine	Inhibited	-2.019	1.63E-04
TLR4	Transmembrane receptor	Inhibited	-2.412	3.93E-04
CD3	Complex	Inhibited	-2.425	1.07E-03
CD44	Other	Inhibited	-2.352	1.27E-03
SYVN1	Transporter	Inhibited	-2.236	1.33E-03
CD24	Other	Inhibited	-2	3.40E-03
LIF	Cytokine	Inhibited	-2.236	8.09E-03
STAT3	Transcription regulator	Inhibited	-2.739	2.37E-02
Pirinixic acid	Chemical toxicant	Inhibited	-2.382	4.24E-02
Insulin	Group	Inhibited	-2.449	5.95E-02
ESR1	Ligand-dependent nuclear receptor	Inhibited	-2.465	1.04E-01

Filter criteria: significant Z-score (≥ 2 for predicted activation and ≤ -2 for predicted inhibition).

Sorting criteria: P value of overlap (analysed by Fisher's Exact Test, IPA).

Supplementary Material

Refer to Web version on PubMed Central for supplementary material.

Acknowledgments

We thank Ulf Hedin and Ljubica Matic for the input on the clinical data. We thank Max Kaller for the assistance with RNA sequencing. We acknowledge the Stanford Cell Science Imaging Facility and Servier Medical Art (www.smart.servier.com) for providing components of Figure 5. This work was supported by the Deutsche Forschungsgemeinschaft (JA 2869/1-1:1 to K.-U.J. and SFB1123 to L.M.); the Deutsche Herzstiftung e.V. (S/09/19 to K.-U.J.); the National Institutes of Health (R35 HL144475 to N.J.L.); the American Heart Association (EIA34770065 to N.J.L.); and the German Centre for Cardiovascular Research (DZHK, Junior Research group to L.M.).

Data availability

The authors declare that all data supporting the findings of this study are available within the paper, its supplementary information files, or publicly available. Raw RNA sequencing data are available from the National Center for Biotechnology Information (NCBI) under accession number PRJNA7337400. Source Data are provided with this paper.

References

1. Virani SS et al. Heart Disease and Stroke Statistics-2021 Update: A Report From the American Heart Association. *Circulation* 143, e254–e743, doi:10.1161/CIR.0000000000000950 (2021). [PubMed: 33501848]
2. Brugs JJ et al. The benefits of statins in people without established cardiovascular disease but with cardiovascular risk factors: meta-analysis of randomised controlled trials. *BMJ* 338, b2376, doi:10.1136/bmj.b2376 (2009). [PubMed: 19567909]
3. Cholesterol Treatment Trialists C et al. Efficacy and safety of more intensive lowering of LDL cholesterol: a meta-analysis of data from 170,000 participants in 26 randomised trials. *Lancet* 376, 1670–1681, doi:10.1016/S0140-6736(10)61350-5 (2010). [PubMed: 21067804]

4. Oesterle A, Laufs U & Liao JK Pleiotropic Effects of Statins on the Cardiovascular System. *Circ Res* 120, 229–243, doi:10.1161/CIRCRESAHA.116.308537 (2017). [PubMed: 28057795]
5. Yu D & Liao JK Emerging views of statin pleiotropy and cholesterol lowering. *Cardiovasc Res*, doi:10.1093/cvr/cvab032 (2021).
6. Ridker PM et al. Rosuvastatin to prevent vascular events in men and women with elevated C-reactive protein. *N Engl J Med* 359, 2195–2207, doi:10.1056/NEJMoa0807646 (2008). [PubMed: 18997196]
7. Dichtl W et al. HMG-CoA reductase inhibitors regulate inflammatory transcription factors in human endothelial and vascular smooth muscle cells. *Arterioscler Thromb Vasc Biol* 23, 58–63, doi:10.1161/01.atv.0000043456.48735.20 (2003). [PubMed: 12524225]
8. Libby P, Ridker PM & Maseri A Inflammation and atherosclerosis. *Circulation* 105, 1135–1143, doi:10.1161/hc0902.104353 (2002). [PubMed: 11877368]
9. Ridker PM et al. Antiinflammatory Therapy with Canakinumab for Atherosclerotic Disease. *N Engl J Med* 377, 1119–1131, doi:10.1056/NEJMoa1707914 (2017). [PubMed: 28845751]
10. Tardif JC et al. Efficacy and Safety of Low-Dose Colchicine after Myocardial Infarction. *N Engl J Med* 381, 2497–2505, doi:10.1056/NEJMoa1912388 (2019). [PubMed: 31733140]
11. Kojima Y et al. CD47-blocking antibodies restore phagocytosis and prevent atherosclerosis. *Nature* 536, 86–90, doi:nature18935 [pii] 10.1038/nature18935 (2016). [PubMed: 27437576]
12. Jarr KU et al. (18)F-Fluorodeoxyglucose-Positron Emission Tomography Imaging Detects Response to Therapeutic Intervention and Plaque Vulnerability in a Murine Model of Advanced Atherosclerotic Disease—Brief Report. *Arterioscler Thromb Vasc Biol* 40, 2821–2828, doi:10.1161/ATVBAHA.120.315239 (2020). [PubMed: 33086865]
13. Flores AM et al. Pro-efferocytic nanoparticles are specifically taken up by lesional macrophages and prevent atherosclerosis. *Nat Nanotechnol* 15, 154–161, doi:10.1038/s41565-019-0619-3 (2020). [PubMed: 31988506]
14. Jarr KU et al. Effect of CD47 Blockade on Vascular Inflammation. *N Engl J Med* 384, 382–383, doi:10.1056/NEJMc2029834 (2021). [PubMed: 33503349]
15. Staffa JA, Chang J & Green L Cerivastatin and reports of fatal rhabdomyolysis. *N Engl J Med* 346, 539–540, doi:10.1056/NEJM200202143460721 (2002).
16. Kolodgie FD et al. Pathologic assessment of the vulnerable human coronary plaque. *Heart* 90, 1385–1391, doi:10.1136/hrt.2004.041798 (2004). [PubMed: 15547008]
17. Roell KR, Reif DM & Motsinger-Reif AA An Introduction to Terminology and Methodology of Chemical Synergy—Perspectives from Across Disciplines. *Front Pharmacol* 8, 158, doi:10.3389/fphar.2017.00158 (2017). [PubMed: 28473769]
18. Kojima Y, Weissman IL & Leeper NJ The Role of Efferocytosis in Atherosclerosis. *Circulation* 135, 476–489, doi:10.1161/circulationaha.116.025684 (2017). [PubMed: 28137963]
19. Schwartz GG et al. Effects of atorvastatin on early recurrent ischemic events in acute coronary syndromes: the MIRACL study: a randomized controlled trial. *JAMA* 285, 1711–1718, doi:10.1001/jama.285.13.1711 (2001). [PubMed: 11277825]
20. Cannon CP et al. Intensive versus moderate lipid lowering with statins after acute coronary syndromes. *N Engl J Med* 350, 1495–1504, doi:10.1056/NEJMoa040583 (2004). [PubMed: 15007110]
21. Bu DX et al. Statin-induced Kruppel-like factor 2 expression in human and mouse T cells reduces inflammatory and pathogenic responses. *J Clin Invest* 120, 1961–1970, doi:10.1172/JCI41384 (2010). [PubMed: 20440076]
22. Sen-Banerjee S et al. Kruppel-like factor 2 as a novel mediator of statin effects in endothelial cells. *Circulation* 112, 720–726, doi:10.1161/CIRCULATIONAHA.104.525774 (2005). [PubMed: 16043642]
23. Weitz-Schmidt G et al. Statins selectively inhibit leukocyte function antigen-1 by binding to a novel regulatory integrin site. *Nat Med* 7, 687–692, doi:10.1038/89058 (2001). [PubMed: 11385505]
24. Laufs U et al. Impact of HMG CoA reductase inhibition on small GTPases in the heart. *Cardiovasc Res* 53, 911–920, doi:10.1016/s0008-6363(01)00540-5 (2002). [PubMed: 11922901]

25. Tanaka S et al. Statins exert the pleiotropic effects through small GTP-binding protein dissociation stimulator upregulation with a resultant Rac1 degradation. *Arterioscler Thromb Vasc Biol* 33, 1591–1600, doi:10.1161/ATVBAHA.112.300922 (2013). [PubMed: 23640485]
26. Ridker PM et al. IL-6 inhibition with ziltivekimab in patients at high atherosclerotic risk (RESCUE): a double-blind, randomised, placebo-controlled, phase 2 trial. *Lancet* 397, 2060–2069, doi:10.1016/S0140-6736(21)00520-1 (2021). [PubMed: 34015342]
27. Tian B et al. Atorvastatin Promotes Phagocytosis and Attenuates Pro-Inflammatory Response in Human Retinal Pigment Epithelial Cells. *Sci Rep* 7, 2329, doi:10.1038/s41598-017-02407-7 (2017). [PubMed: 28539592]
28. Tanaka N, Abe-Dohmae S, Iwamoto N, Fitzgerald ML & Yokoyama S HMG-CoA reductase inhibitors enhance phagocytosis by upregulating ATP-binding cassette transporter A7. *Atherosclerosis* 217, 407–414, doi:10.1016/j.atherosclerosis.2011.06.031 (2011). [PubMed: 21762915]
29. Holschermann H et al. Statins prevent NF-kappaB transactivation independently of the IKK-pathway in human endothelial cells. *Atherosclerosis* 185, 240–245, doi:10.1016/j.atherosclerosis.2005.06.019 (2006). [PubMed: 16051251]
30. Vallejo AN, Yang H, Klimiuk PA, Weyand CM & Goronzy JJ Synovocyte-mediated expansion of inflammatory T cells in rheumatoid synovitis is dependent on CD47-thrombospondin 1 interaction. *J Immunol* 171, 1732–1740, doi:10.4049/jimmunol.171.4.1732 (2003). [PubMed: 12902472]
31. Fortin G et al. A role for CD47 in the development of experimental colitis mediated by SIRPalpha+CD103- dendritic cells. *J Exp Med* 206, 1995–2011, doi:10.1084/jem.20082805 (2009). [PubMed: 19703989]
32. Shi L et al. CD47 deficiency ameliorates autoimmune nephritis in Fas(lpr) mice by suppressing IgG autoantibody production. *J Pathol* 237, 285–295, doi:10.1002/path.4574 (2015). [PubMed: 26095930]
33. Delsing DJ et al. Differential effects of amlodipine and atorvastatin treatment and their combination on atherosclerosis in ApoE*3-Leiden transgenic mice. *J Cardiovasc Pharmacol* 42, 63–70, doi:10.1097/00005344-200307000-00010 (2003). [PubMed: 12827028]
34. Grothusen C et al. Combined effects of HMG-CoA-reductase inhibition and renin-angiotensin system blockade on experimental atherosclerosis. *Atherosclerosis* 182, 57–69, doi:10.1016/j.atherosclerosis.2005.01.045 (2005). [PubMed: 16115475]
35. Lee SG et al. Synergistic protective effects of a statin and an angiotensin receptor blocker for initiation and progression of atherosclerosis. *PLoS One* 14, e0215604, doi:10.1371/journal.pone.0215604 (2019). [PubMed: 31050669]
36. Advani R et al. CD47 Blockade by Hu5F9-G4 and Rituximab in Non-Hodgkin's Lymphoma. *N Engl J Med* 379, 1711–1721, doi:10.1056/NEJMoa1807315 (2018). [PubMed: 30380386]
37. Afgan E et al. The Galaxy platform for accessible, reproducible and collaborative biomedical analyses: 2018 update. *Nucleic Acids Res* 46, W537–W544, doi:10.1093/nar/gky379 (2018). [PubMed: 29790989]
38. Nicoletti A, Kaveri S, Caligiuri G, Bariety J & Hansson GK Immunoglobulin treatment reduces atherosclerosis in apo E knockout mice. *J Clin Invest* 102, 910–918, doi:10.1172/JCI119892 (1998). [PubMed: 9727059]

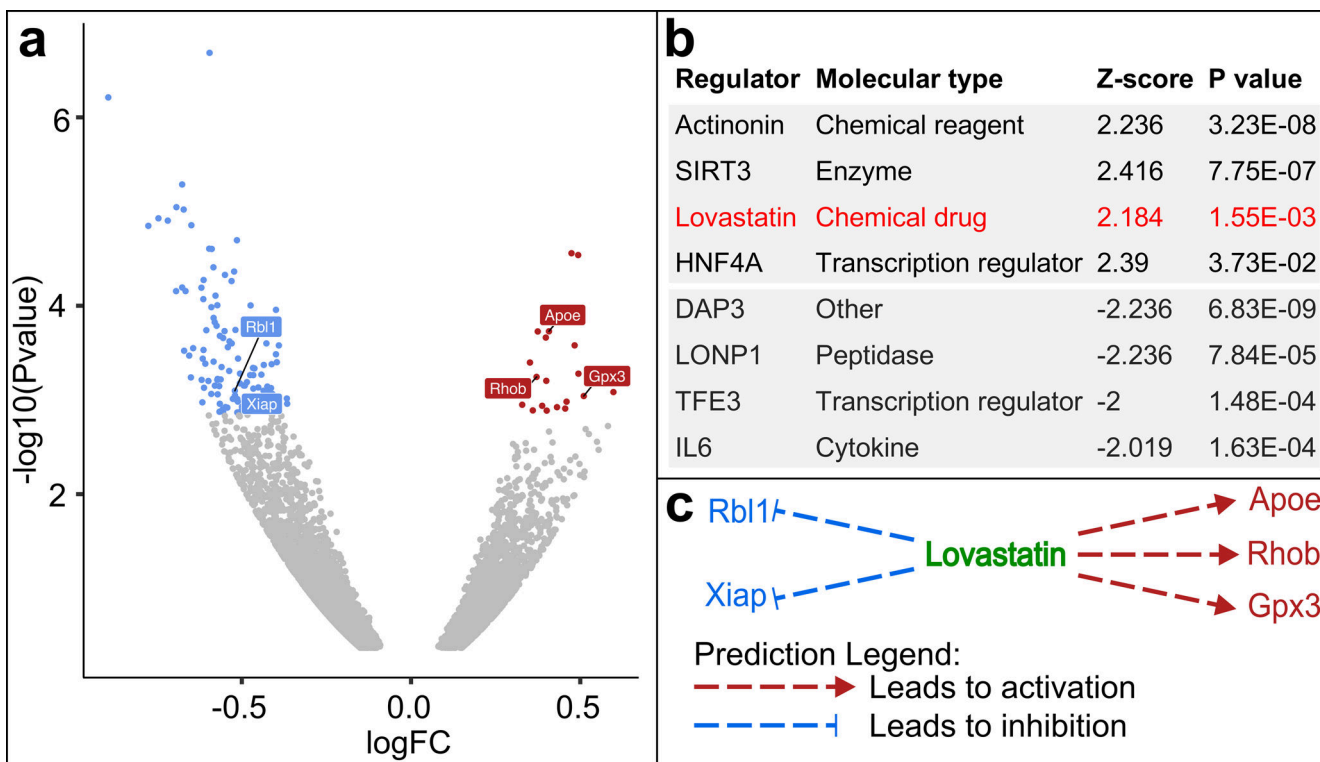


Figure 1: RNA sequencing revealed HMG-CoA reductase inhibitor as one of the top upstream regulators of SHP-1 inhibition in macrophages.

a, Volcano plot of genes that regulate the response to SHP1i in bone marrow-derived macrophages ($n = 3$ biologically independent samples per group). Significant hits were defined by a false-discovery rate < 0.10 and marked in blue (downregulated) or red (upregulated). FC, fold change; Rbl1, RB transcriptional corepressor like 1; Xiap, X-linked inhibitor of apoptosis; Apoe, apolipoprotein E; Rhob, ras homolog family member B; Gpx3, glutathione peroxidase 3. **b – c**, Lovastatin, a first generation HMG-CoA reductase inhibitor, was one of the top activated upstream regulators and the only drug in the database, based on the relevant regulation of Apoe, Rhob, Rbl1, Gpx3, and Xiap. Filter criteria: top four upstream regulators with significant Z-score (≥ 2 for predicted activation and ≤ -2 for predicted inhibition). Sorting criteria: P value of overlap analysed by Fisher’s Exact Test, IPA.

All false-discovery rate values are provided in Extended Data Table 1. All significant upstream regulators (Z-score ≥ 2 for predicted activation and ≤ -2 for predicted inhibition) are provided in Extended Data Table 2.

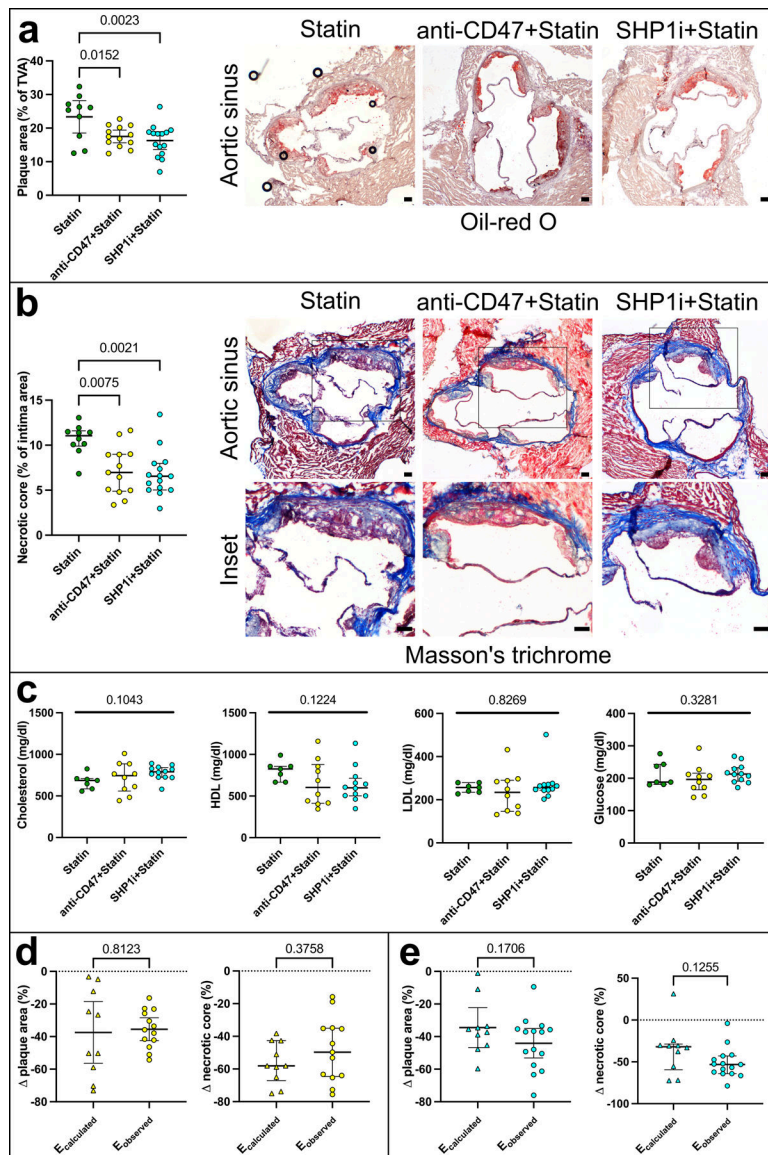


Figure 2: Combined treatment of CD47-SIRP α blockade and atorvastatin showed additive effects on atherosclerotic plaque activity *in vivo*.

a, Quantification of atherosclerotic lesion area and cross-sections of aortic roots stained with Oil-red O ($n = 10$ for Statin; $n = 13$ for anti-CD47+Statin; $n = 15$ for SHP1i+Statin). TVA, total vessel area; Scale bar, 100 μm . **b**, Quantification of necrotic core size and cross-sections of aortic roots stained with Masson's trichrome ($n = 10$ for Statin; $n = 13$ for anti-CD47+Statin; $n = 15$ for SHP1i+Statin). Scale bar and scale bar inset, 100 μm . **c**, Quantification of total cholesterol, high-density lipoprotein (HDL), low-density lipoprotein (LDL), and glucose in the blood ($n = 7$ for Statin; $n = 10$ for anti-CD47+Statin; $n = 12$ for SHP1i+Statin). **d – e**, Applying the Bliss independence model on the analyses of lesion area and necrotic core size to determine additivity/synergy of compounds ($n = 10$ for $E_{\text{calculated}}$; $n = 13$ for anti-CD47+Statin E_{observed} ; $n = 15$ for SHP1i+Statin E_{observed}). Δ , change in. Each data point represents a biologically independent animal. Data and error bars present mean \pm 95 % confidence interval for parametric and median \pm interquartile range for

non-parametric results. Data of **(a)** were analysed by one-way analysis of variance with Sidak's multiple comparisons test. Data of **(b – c)** were analysed by Kruskal-Wallis with Dunn's multiple comparisons test. Data of **(d – e)** were analysed by unpaired Student's *t*-test (two-tailed) and Mann–Whitney *U* test (two-tailed).

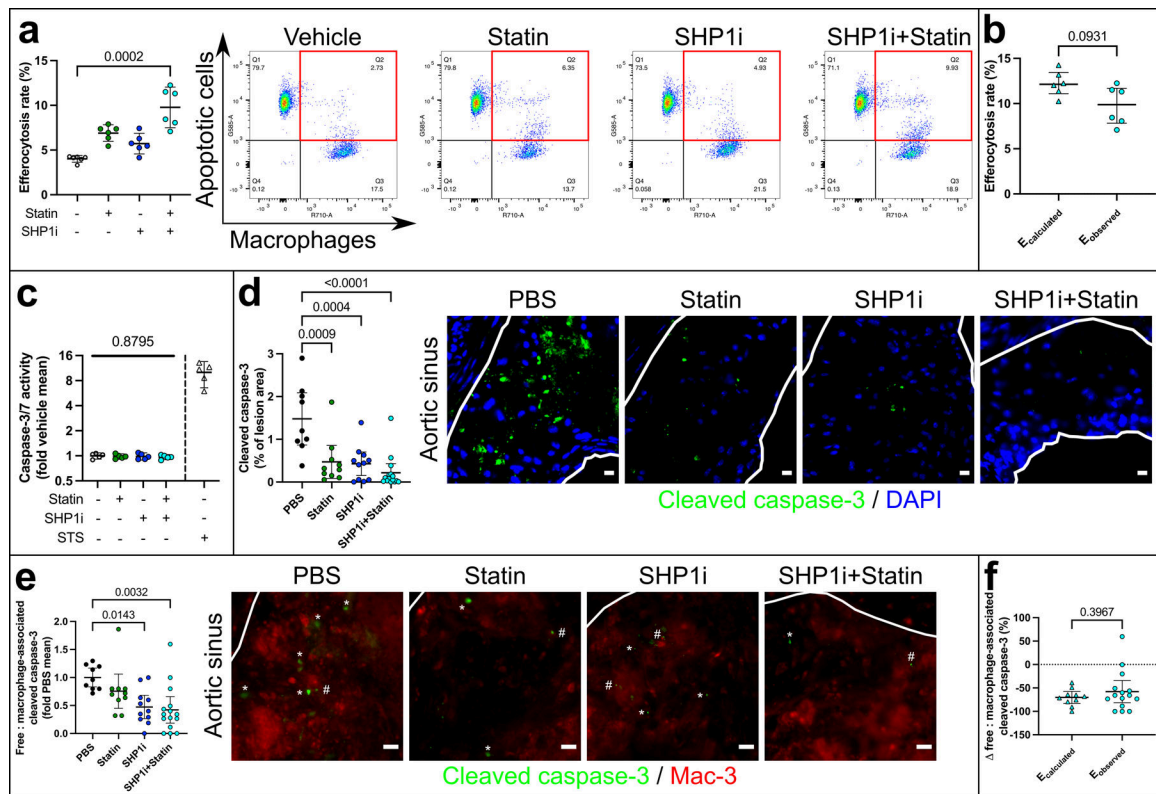


Figure 3: Combined treatment of CD47-SIRP α blockade and atorvastatin showed additive effects on efferocytosis rate *in vitro* and *in vivo*.

a, Quantification of efferocytosis rate and flow cytometry plots depicting the efferocytosis rate *in vitro* in the presence or absence of atorvastatin, SHP1i, and dual treatment ($n = 6$ biologically independent samples per group). The right upper quadrant (highlighted in red) includes double-positive cells that are taken to represent a macrophage that has ingested an apoptotic target cell. **b**, Applying the Bliss independence model on the analyses of efferocytosis rate *in vitro* to determine additivity/synergy of compounds ($n = 6$ biologically independent samples per group). **c**, Apoptosis assay to quantify the rate of programmed cell death *in vitro* in the presence or absence of atorvastatin, SHP1i, and dual treatment ($n = 5$ biologically independent samples per group). STS, staurosporine. **d**, Quantification of cleaved caspase-3 activity and immunofluorescence images ($n = 9$ for PBS; $n = 10$ for Statin; $n = 11$ for SHP1i; $n = 15$ for SHP1i+Statin). White line depicts intima. Scale bar, 10 μm . **e**, Quantification of efferocytosis rate *in vivo* and immunofluorescence images depicting the ratio of free to macrophage associated cleaved caspase-3 activity ($n = 9$ for PBS; $n = 10$ for Statin; $n = 11$ for SHP1i; $n = 15$ for SHP1i+Statin). White line depicts intima. *, free cleaved caspase-3. #, macrophage-associated cleaved caspase-3. Scale bar, 10 μm . **f**, Applying the Bliss independence model on the analyses of efferocytosis rate *in vivo* to determine additivity/synergy of compounds ($n = 10 E_{\text{calculated}}$; $n = 15 E_{\text{observed}}$). Δ , change in.

Each data point represents a biologically independent sample or animal. Data and error bars present mean \pm 95 % confidence interval for parametric and median \pm interquartile range for non-parametric results. Data of **(a)** were analysed by Kruskal-Wallis with Dunn's

multiple comparisons test. Data of **(b)** were analysed by Mann–Whitney *U* test (two-tailed). Data of **(c – e)** were analysed by one-way analysis of variance with Tukey’s multiple comparisons test. Data of **(f)** were analysed by unpaired Student’s *t*-test (two-tailed).

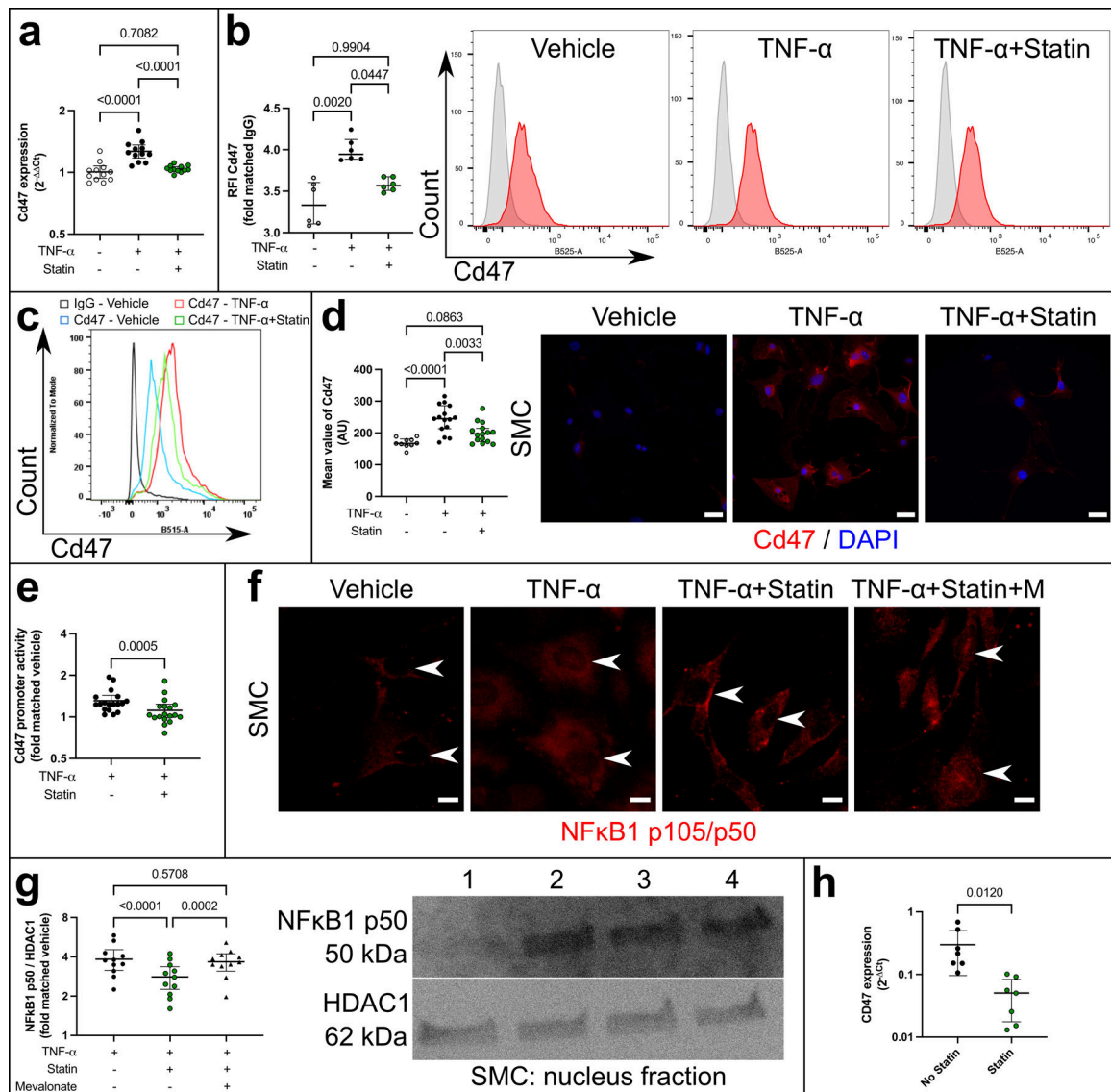


Figure 4: Atorvastatin inhibited NFκB1 p50 nuclear translocation under atherogenic conditions and thus directly regulated gene expression of Cd47.

a, Cd47 expression by quantitative polymerase chain reaction in smooth muscle cells ($n = 12$ biologically independent samples per group). TNF- α , tumor necrosis factor- α . **b – c**, Cd47 expression by flow cytometry in smooth muscle cells ($n = 6$ biologically independent samples per group). RFI, ratio of median fluorescence intensity. **d**, Cd47 expression by immunofluorescence in smooth muscle cells ($n = 10$ cells for vehicle and $n = 15$ cells for TNF- α or TNF- α +Statin examined over 3 biologically independent samples per group). AU, arbitrary unit. SMC, smooth muscle cells. Scale bar, 10 μ m. **e**, Cd47 promoter activity by luciferase assay in smooth muscle cells ($n = 18$ biologically independent samples per group). **f**, NFκB1 p50 nuclear translocation by immunofluorescence in smooth muscle cells ($n = 3$ biologically independent samples per group). NFκB1, nuclear factor of kappa light polypeptide gene enhancer in B cells 1. M, mevalonate. Scale bar, 10 μ m. **g**, NFκB1 p50 nuclear translocation by Western blot in smooth muscle cells ($n = 11$ biologically

independent samples per group). HDAC1, histone deacetylase 1. Lane 1, Vehicle. Lane 2, TNF- α . Lane 3, TNF- α +Statin. Lane 4, TNF- α +Statin+Mevalonate. **h**, CD47 expression by quantitative polymerase chain reaction in carotid endarterectomy samples ($n = 7$ biologically independent samples per group).

Each data point represents a biologically independent sample, except for (**d**), which shows cells examined (mean value per high power field) over 3 biologically independent samples. Data and error bars present mean \pm 95 % confidence interval for parametric and median \pm interquartile range for non-parametric results. Data of (**a**) and (**d**) were analysed by one-way analysis of variance with Tukey's multiple comparisons test. Data of (**b**) were analysed by Kruskal-Wallis with Dunn's multiple comparisons test. Data of (**e**) were analysed by paired Student's *t*-test (two-tailed). Data of (**g**) were analysed by repeated measures analysis of variance with Tukey's multiple comparisons test. Data of (**h**) were analysed by unpaired Student's *t*-test (two-tailed).

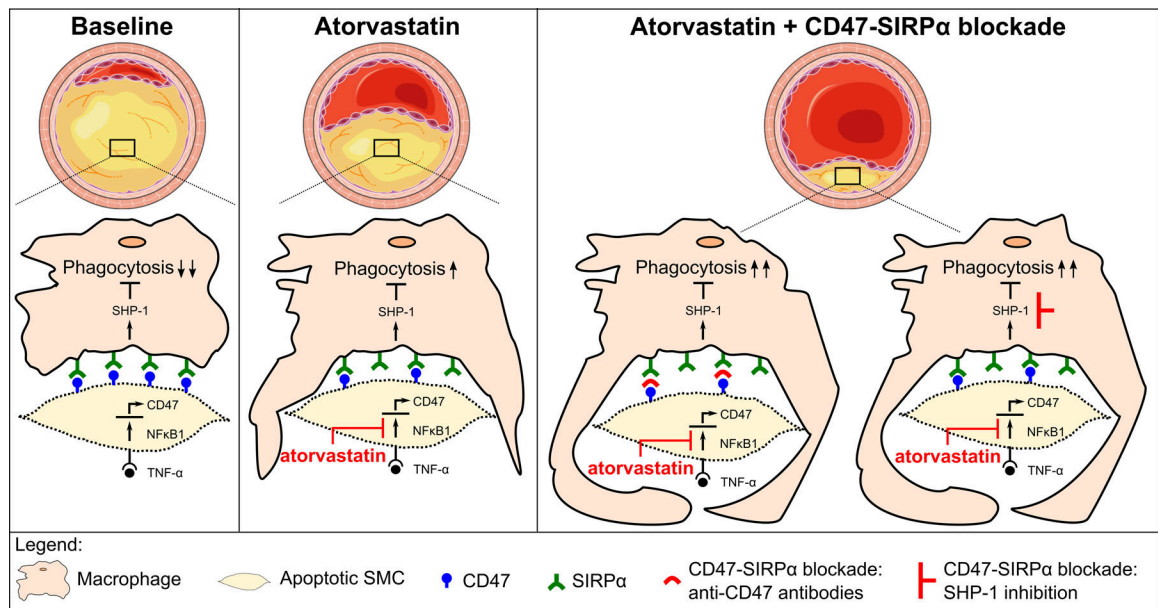


Figure 5: The pleiotropic benefits of statins include the activation of efferocytosis in atherosclerosis.

In advanced atherosclerotic lesions, atorvastatin augments efferocytosis by inhibiting the nuclear translocation of NF κ B1 p50 and suppressing expression of the key ‘don’t eat me’ molecule CD47 in vascular smooth muscle cells. Combination of HMG-CoA reductase inhibition and CD47-SIRP α blockade amplifies the phagocytic capacity of macrophages and thus prevents lesion progression in an additive manner. SHP-1, Src homology 2 domain-containing phosphatase-1. SIRP α , signal-regulatory protein alpha.